SONNE-Berichte

A high-resolution controlled-source seismic experiment offshore Taltal to elucidate structural controls on megathrust slip

Cruise No. SO297

February 23 – April 11, 2023,
Talcahuano (Chile) – Guayaquil (Ecuador)
PISAGUA

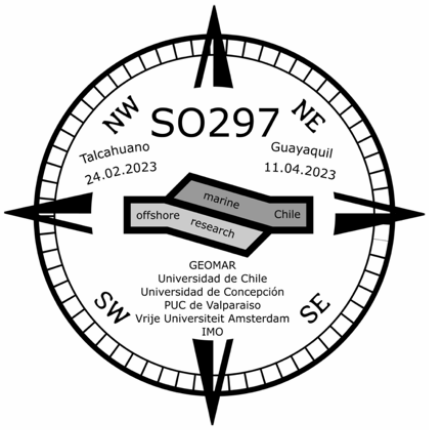

D. Lange, H. Kopp, A. Dannowski, I. Klaucke, M. Moreno, J. Diaz, M. Kühn, M. Riedel, E. Contreras-Reyes and all cruise participants

D. Lange
GEOMAR Helmholtz Centre for Ocean Research Kiel

2023

Table of Contents

1 Cruise Summary

1.1 Summary in English

The main objective of the PISAGUA project is a detailed high-resolution model of the marine forearc in Northern Chile. The 2D and 3D refraction seismic experiment offshore Taltal was designed to investigate the control of the plate margin structures on earthquake rupture behavior. A significant region of previously uncharted seafloor at latitudes of the Taltal ridge and Copiapó ride was mapped with multibeam for the first time. The multibeam mapping revealed significant west-east oriented normal faulting in the region of the incoming Taltal ridge. Furthermore, we installed five novel drift-free pressure sensors (A-0-A type) to resolve subsidence and sea-level changes with a precision better than 1 cm for over five years. The offshore observations were complemented in December 2022 with 24 short-period seismometer stations installed from the Instituto Milenio de Oceanografía (IMO) and 30 seismometers installed from GEOMAR in February 2023. During the cruise, 42 ocean bottom seismometers and hydrophones from the GEOMAR pool were deployed a total of 115 times for two seismic refraction profiles and one 3D experiment. Overall, all objectives of the cruise were accomplished.

1.2 Zusammenfassung

Das Hauptziel des PISAGUA-Projekts ist ein detailliertes, hochauflösendes Modell des marinen Forearcs in Nordchile. Das 2D- und 3D-refraktionsseismische Experiment vor der Küste von Taltal wurde konzipiert, um die Kontrolle der Plattenrandstrukturen über das Bruchverhalten bei Erdbeben zu untersuchen. Die Fächerecholotkartierung zeigte eine signifikante west-östlich orientierte Normalverwerfung in der Region des ankommenden Taltal-Rückens. Darüber hinaus installierten wir fünf neuartige driftfreie Drucksensoren (Typ A-0-A), um über fünf Jahre hinweg Senkungen und Meeresspiegelveränderungen mit einer Genauigkeit von mehr als 1 cm aufzulösen. 24 kurzperiodische Seismometerstationen des Instituto Milenio de Oceanografía (IMO) im Dezember 2022 und 30 Seismometer des GEOMAR im Februar 2023 ergänzten die Offshore-Beobachtungen an Land. Während der Fahrt wurden 42 Ozeanbodenseismometer und Hydrophone aus dem GEOMAR-Pool insgesamt 115 mal für zwei seismische Refraktionsprofile und ein 3D-Experiment eingesetzt. Insgesamt wurden alle Ziele der Fahrt erreicht.

2 Participants

2.1 Principal Investigators

Name	Institution
Lange, Dietrich, Dr.	GEOMAR
Kopp, Heidrun, Prof. Dr.	GEOMAR

2.2 Scientific Party

Tab. 2.1 List of scientific cruise participants in alphabetic order.

Name	Discipline	Institution
Bartels, Thies	Airgun/Streamer/OBS	GEOMAR
Bauer, Benedikt	OBH/OBS	GEOMAR
Beniest, Anouk, Prof.	OBH/OBS	Vrije Universiteit Amsterdam
Carillo Barra, Vanessa	OBH/OBS	FCFM, Universidad de Chile
Contreras Reyes, Eduardo, Prof.	Multibeam	FCFM, Universidad de Chile
Cristosto Urrutia, Lucas	Multibeam	Universidad de Concepción
Dannowski, Anke, Dr.	OBH/OBS	GEOMAR
Diaz, Juan, Prof.	pressure sensors	Pontificia Universidad Catolica de Valparaiso
Donoso Urrutia, Felipe	pressure sensors	Universidad de Concepción
Filbrandt, Christian	Airgun/Streamer/OBS	GEOMAR
Kopp, Heidrun, Prof. Dr.	Co-Chief Scientist	GEOMAR
Jegen, Anna	OBH/OBS	GEOMAR
Kahler, Merit	OBH/OBS	GEOMAR
Klaucke, Ingo, Dr.	Bathymetry	GEOMAR
Kuehn, Michel	MCS / Streamer	GEOMAR
Kuntze, Alina	OBH/OBS	GEOMAR
Lange, Dietrich, Dr.	Chief Scientist	GEOMAR
Moreno, Marcos, Prof.	pressure sensors	IMO
Murray-Bergquist, Louisa	OBH/OBS	GEOMAR
Obando Orrego, Sebastian	OBH/OBS	Universidad de Chile
Pinto Juica, Mauro	pressure sensors	Universidad de Concepción/IMO
Pries, Stephan	OBH/OBS	GEOMAR
Riedel, Michael, Dr.	OBH/OBS	GEOMAR
Rohde, Lea	Airgun/ Streamer/OBS	GEOMAR
Schaefer, Wiebke	OBH/OBS	GEOMAR
Schaetzel, Julia	OBH/OBS/Multibeam	GEOMAR
Search Toloza, Francesca	Observer	SHOA
Urrutia, Isabel	pressure sensors	Universidad de Concepción
Wallner, Ole	OBH/OBS	GEOMAR
Warwel, Arne	OBH/OBS	GEOMAR
Wegehaupt , Swantje	OBH/OBS/Multibeam	GEOMAR

2.3 Participating Institutions

- GEOMAR Helmholtz-Zentrum für Ozeanforschung Kiel, Germany
- Universidad de Chile, Chile
- Universidad de Concepcion, Chile
- Vrije Universiteit Amserdam, Niederlande
- Instituto Milenio de Oceanografía, Chile
- Pontificia Universidad Católica de Valparaíso, Chile

3 Research Program

3.1 Description of the Work Area

Subduction zones outline much of the Pacific plate, producing many of the largest and most destructive earthquakes recorded (e.g., Bilek, 2010). During great earthquakes (M>8) along these convergent plate boundaries, the shallow interface between the plates ruptures down to depths of up to 50 km (e.g., Oleskevich et al., 1999), while the rupture propagates laterally along the margin. The properties of the plate interface are heterogeneous, and this is reflected by the complex pattern of coupling between the plates, coseismic slip distributions and afterslip related to postseismic deformation.

Subduction zones are usually classified as either erosional, where the material is removed from the base of the overriding plate, or accretionary, with material actively added to the overriding plate. Although 57% of worldwide subduction zones are erosive, much of the early research on subduction zone dynamics focused on accretionary margins (Bilek, 2010). Large subduction zone earthquakes (M>9) were suggested to occur in accretionary margins, while tsunami earthquakes (i.e. earthquakes that generate disproportionately large tsunamis for the given magnitude due to long rupture durations) have occurred primarily in erosional margins (Bilek, 2010). However, the Mw=9.0 2011 Tohoku earthquake did not follow these previous observations since it occurred on an erosive margin rupturing the seismogenic zone and up-dip to the trench axis in a single great event, which was not observed since instrumental observation. Equally, the tsunami earthquake along the accretionary Sumatran margin with a moment magnitude of Mw 7.7 on 25 October 2010 (Collings et al., 2012) resulted in a tsunami with runups over 7 m height in the nearfield.

The Chilean margin was the site of several recent large megathrust earthquakes recorded *onshore* on modern, high-resolution seismic and geodetic instrumentation, yielding detailed information on the history of slip on the plate boundary before, during and after the earthquake. Because of this rich earthquake history and the systematic spatial variation in geologic factors that potentially affect megathrust deformation, the Chile subduction zone is arguably the best place on Earth to understand the effect of crustal structure and sedimentation on the behavior of continent-ocean subduction plate boundaries. However, a similar effort has not targeted the *offshore* domain and hence the location of the seismogenic zone.

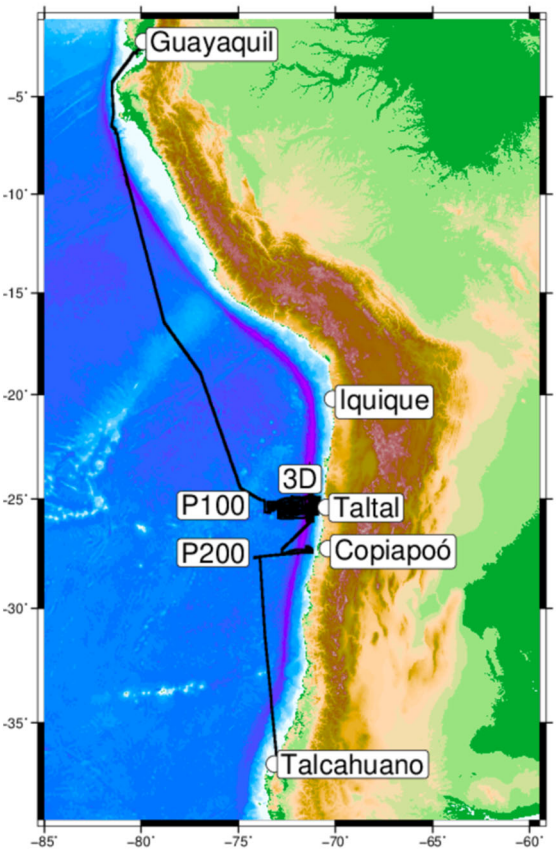

Fig. 3.1 Track chart of RV SONNE cruise SO297. Bathymetry from Smith and Sandwell (1997). The working areas were offshore Copiapó (27°35'S) for refraction profile P200 and offshore Taltal for refraction profile P100 (at 25°22'S). Furthermore, an anisotropy experiment on the oceanic plate and a large 3D refraction experiment were conducted offshore Taltal. Bathymetry and Topography from GEBCO.

The working regions offshore Taltal and Copiapó were last affected by the 1922 Atacama earthquake (Mw 8.8). The 1922 earthquake ruptured the plate interface between 26°S and 30ºS and caused a tsunami. The 1922 earthquake had a complex source time function with three pulses of quick moment release during the 76-second duration. This complex source function indicates heterogeneities of the plate interface. The following tsunami was observed as far as Lima/Callao in Peru (e.g., Beck et al., 1998). As a result, the shallow part of the plate boundary between 23°S and 26°S remains unbroken and thus probably represents a seismic gap.

Although the area is currently in the interseismic phase of the earthquake cycle, the background activity is significant. Ten earthquakes with magnitudes above 6.5 have occurred since 1970 (Antofagasta and 700 km south). The last one was on 1 September 2020 offshore Vallenar (28°S) with a moment magnitude of 6.8.

The largest earthquake during the SO297 cruise was an Mw 5.9 earthquake on 04 April 2023 at 19:08:47 (UTC), very close to the coast (70.77°W 27.42°S) on the prolongation of profile P200 and likely just within our network of land stations which were installed jointly by IMO and GEOMAR to register the airgun shots onshore. The focal mechanism was oblique extensional (http://geofon.gfz-potsdam.de/eqinfo/event.php?id=gfz2023gpjr).

The station coverage of northern Chile has greatly improved due to the densification of the land network (GPS, seismometers) by the Chilean authorities (http://ds.iris.edu/gmap/#network=C1). This densification will lead to improved coupling models for the region.

Although several 2D refraction profiles are known for northern and southern Chile (northern Chile: Sallarès and Ranero, 2005; Contreras-Reyes et al., 2012, Tréhu, et al., 2016; southern Chile: seven profiles, Fig. 3 in Contreras-Reyes, 2018), a gap of 825 km (between 23.5°S, Mejillones Peninsula and 31°S Puntaqui) remains without information on the structure of the marine forearc

(Contreras-Reyes, 2018). Further knowledge of Chile's marine forearc is based on tomographic inversion of earthquake data, but for the Taltal and Copiapó regions, information on the velocity structure remains sparse.

Only the reflection lines of RV SONNE cruise SO104/CINCA from 1995 (Reichert et al., 1996) provide information about the marine forearcs in the SO297 working area. Similarly, high-resolution bathymetry offshore Taltal is only partly available in the SO297 working area. A part of the marine forearc at 25°S was mapped during SO288 (Kopp et al., 2022) in order to identify good locations for the absolute pressure sensors. A smaller area around the deepest part of the Atacama Trench (8066 m) was surveyed with EM122 by Victor Vescovo and Osvaldo Ulloa (Universidad de Concepción) for the preparations of the manned Atacama Deep Trench dive on 21 January 2022. The rest of the area offshore Taltal is only known from a limited number of multibeam measurements during transits of FS SONNE or from the SO104/CINCA cruise (Reichert et al., 1996).

3.2 Aims of the Cruise

The objective of cruise SO297 was to investigate in detail the deep structure offshore Taltal and Copiapó with 2D and 3D refraction experiments to analyze the relationship between deformation behavior and forearc structures using the northern Chilean subduction zone as a type location. This work will contribute to regional hazard studies. For a better understanding of the processes, the required knowledge of the deep structure of the marine forearc and the seismogenic zone is lacking to date since this seaward region has not been investigated with modern technology. Therefore, the SO297 high-resolution dataset for the marine forearc in Northern Chile will, for the first time, image the forearc of the erosional subduction zone offshore Taltal and Copiapó.

The main theme is the relation of forearc structures on the forearc deformation of an erosive margin during the inter-seismic phase, including its along strike and downdip segmentation in a region where dense geophysical datasets from land observations are available. Associated with this theme are:

a.) the seismotectonic setting of the study area,
b.) the velocity structure of the forearc, including the structure of the oceanic plate,
c.) the internal structure of the forearc for both down-dip and lateral changes,
d.) the structural control on megathrust deformation during the seismic cycle's co-seismic, inter-seismic, and post-seismic phases.

Generally, the controlling factors on asperities and deformation along the subducting interface are suggested to be governed by the structure and physical properties of the subducting and overriding plates, respectively. In detail, these key controls are related to:

a.) The structure and geometry of the subducted **incoming oceanic plate,** such as the plate roughness, the sea floor age, the trench sediment fill (Kopp, 2013, and references therein), the convergence velocity/obliquity, the temperature field (e.g. Oleskevich et al., 1999), slab geometry (Contreras-Reyes et al., 2012) and additional parameters (Kanamori, 1986, and references therein).
b.) The structure and properties of the **overriding continental plate**.
c.) **Frictional properties** along the subduction interface (e.g., Moreno et al., 2014), including megathrust contact geometry and subduction channel (e.g., Contreras-Reyes & Carrizo, 2011).

By comparing slip models from geodetic and seismological data (e.g., co-seismic and afterslip models or inter-seismic coupling information) with wide-angle refraction results can resolve a.) and b.) may be resolved. Additionally, the offshore data will be complemented by land observations of the IPOC (Integrated Plate Boundary Observatory Chile) network, the ANILLO project and permanent stations from the Centro Sismológico National (CSN).

Overall, the datasets acquired during SO297 will be used to contribute to the following three hypotheses:

Hypothesis 1: The structural properties of the upper plate determine the upper (seaward) boundary of the seismogenic zone and, thus the rupture size of tsunamigenic earthquakes (e.g. Sallarès and Ranero, 2019).

Hypothesis 2: The coupling properties perpendicular as well as parallel to the deep-sea trench are determined by areas that differ in their frictional properties. The geometry of these rupture regions (asperities) can be mapped by high-resolution refraction-seismic imaging methods and is also likely to be determined by velocity contrasts in the oceanic plate.

Hypothesis 3: The high seismic coupling and associated segmentation of the marine subduction zone have been associated with structural and geometric heterogeneities. Such heterogeneities are caused e.g. by subducted seamount chains or deep-sea mountains and can be identified with wide-angle refraction methods.

3.3 Agenda of the Cruise

During the cruise, we installed and acquired a 295 km long seismic refraction profile P200 with 39 OBS/OBH at latitudes of Copiapó. Furthermore, we installed 42 OBS/OBH for a 3D refraction experiment. 9 OBS of the three-dimensional experiment could be used for the 248 km long seismic refraction profile P100 at latitudes of Taltal, followed by an anisotropy refraction experiment with 5 OBS/OBH. A total distance of 2151 km of refraction profiles (with the MCS streamer) was acquired, and 228 km with a configuration optimized for the MCS streamer. In total, 42 OBS/OBH were installed 116 times. Two OBH could not be recovered.

Prior to triggering the seismic sources with a soft start and in daylight and adequate visibility, a mitigation radius of 750 m was visually scanned for marine mammals for a period of 60 s. Measurements only commenced when no marine mammals were observed within the mitigation radius. The mitigation radius was continuously monitored during the entire measurement. Measurements were immediately stopped if mammals were observed in the mitigation radius and were only continued after the animals had left the zone. If measurements were interrupted for more than 10 minutes, they were re-started with a soft start.

During the cruise SO297 a significant volume of EM122 Multibeam and PARASOUND data was acquired. The approximate length of hydroacoustic mapping is ~4200 km. The EM122 multibeam survey covered 38.200 km^2 of the marine forearc and incoming oceanic plate. The EM122 multibeam data was fully processed during the cruise.

Furthermore, five novel absolute pressure instrument moorings (three from IMO and two from GEOMAR) were installed between 1785 m and 5961 m water depth using the deep-sea cable of RV SONNE. The absolute pressure sensors will remain on the seafloor for 2 (5) years for the GEOMAR (IMO) stations, respectively.

Four CTD sound velocity profiles were obtained until 2500 m water depth. No samples were taken during the cruise, and only digital data were obtained.

4 Narrative of the Cruise

Throughout the cruise weather conditions were optimal, always calm seas and no rain.

On Thursday, 23 February, at 12:30, FS SONNE departed San Vicente a day earlier than planned in very calm seas to bunker overnight at Talcahuano (Fig. 3.1) – roadstead - near Quiriquina Island. Four containers were already aboard FS SONNE from previous sailings, and two more containers from Kiel were picked up during the port call by FS SONNE. Immediately after embarkation, we started unpacking the boxes and setting up the labs in the late afternoon.

During the three-day transit to our first working area offshore Copiapó (Fig. 3.1), the Ocean Bottom Seismometers (OBS), Ocean Bottom Hydrophones (OBH), releasers, airguns, multichannel seismic (MCS) streamer and pressure sensors were prepared, and safety briefings were conducted.

The transit was interrupted by releaser tests during the night of February 25-26 after 350 nautical miles of northbound travel. All 44 releasers functioned as desired. One releaser test was performed on the CTD rosette to obtain the first sound velocity profile (Fig. 11.7).

The remaining 20 hours of transit to the first seismic profile were characterized by intensive preparations for the deployment of a total of 39 OBS and OBH on profile P2.

We began deploying stations on P200 at a station spacing of 3.8 nautical miles on 27 February. After deploying 29 stations, a CTD was run at 14:00 to obtain a water sound velocity profile. The deployment of the stations continued until 02:00 on 28 February. At one station the floating line got caught under the OBS. This unit was immediately released, a new anchor attached and was reinstalled after a short time. In the morning of the 28 February RV SONNE mapped the marine forearc with multibeam bathymetry and in the afternoon, the air pulsers and MCS streamer were launched and marine mammal mitigation measures were started. Throughout the cruise, marine mammal mitigation procedures were followed prior to and during the shooting.

Acquisition of the profile lasted until 08:00 on 2nd March. After retrieval of the air pulsers and the MCS streamer, we started dismantling the stations. After the successful recovery of 17 OBS/OBH, one OBH (station P217) surfaced very slowly to finally be located at a constant water depth of 590 meters. After three hours of waiting, we decided to recover two more OBS and returned to P217 after another four hours. OBH P217 continued to ascend very slowly. After triangulating the station using acoustic distance measurements in the water, we determined the remaining station depth to be 530 m and a slow drift to the south. We continued to dismantle the other stations on profile P2. One station, which was installed between two large seamounts and was released at 18:48, drifted very quickly with peak speeds between 1 m/s and 2 m/s from to the southwest. Despite the high drift velocity and two changes of direction of the OBS drift, the OBS was recovered at 00:22 on 04 March at a distance of 3.5 nautical miles from the deployment point. The successful recovery of the remaining stations was completed by the evening of 04 March. On the night of 5 March, we returned to OBH P217 and charted previously unmapped seabed during the transit. We reached the installation position at 06 am, but could not receive any visual or acoustic signals from the station and unfortunately had to leave this station site without OBH P217. We continued northeast to reach the first station of the 3D experiment and performed a releaser test and two float tests during the 12-hour transit (Fig. 3.1).

Deployment of the 3D experiment started on 05 March at 23:30 and ended on 07 March at 17:00. A total of 42 OBS and OBH were deployed over an area of 85 x 50 nautical miles (Fig. 5.5). On 6 March and in the central area of the 3D experiment, a CTD with a releaser test and a float test for the frames of the drift-free pressure sensors to be installed later during SO297 were carried out. After deploying the last OBH, the air pulsers were launched starboard and port side, and the acquisition of the 3D refraction data including the MCS streamer started. At 11 am on Wednesday, 15/03, the air pulsers and streamer were retrieved to perform equipment maintenance. Then, after a short transit of 14 nautical miles, the southernmost station in the network (OBS 3B13) was recovered. At 2 pm, FS SONNE headed west to survey unmapped seafloor on the oceanic plate. At 4 pm, we mapped parts of a seamount that rises well above the surrounding seabed (Fig. 5.1). The multibeam survey ended at 04:45 on 17/03 at the position of the first drift-free pressure sensor from IMO (Fig. 11.5). The installation of the drift-free of pressure sensor PRS1 from IMO in 1774 m water depth started after a CTD (17/03, 04:45) to obtain a water velocity sound profile. First, an acoustic modem was lowered to 50 m water depth. Then, the pressure sensor PRS1 was lowered on the deep-sea wire to the seafloor. The instrument reached the seafloor at 10:51. Details on the installation procedure are shown in Fig. 11.8. After releasing the instrument, it turned out that the instrument was still attached to the cable, as the depth of the instrument decreased when the cable was uplifted. We hoisted the pressure sensor with its frame to the sea surface. When the instrument reached the sea surface (12:39), we saw that the lines were jammed in the device, but the releaser had been triggered. As it was hoisted above the water surface, the weight of the pressure sensor was sufficient to release the lines. The device returned to the seabed with a fall speed of 1 m/s. During its decent, we were connected to the device and could measure the distance and check the status of the device via an acoustic connection at any time. By 13:07 am, it had arrived at 1785 m water depth, standing almost horizontally with an angle of incidence of two degrees. An upload of the data from the device on the seabed showed that the pressure sensor was working as desired.

After a short transit, the air pulsers and streamer were launched at 17:00, and a refraction profile was run through the network to the southernmost point and then back north until the morning after next (19/03, 07:00). The MCS streamer was retrieved at 09:00 on 18/03 as it was not working correctly. The air pulsers remained in the water.

On the morning of 19/03, we installed the second pressure sensor at ~25°S at a planned water depth of 5943 m. Below 5600 m, we suddenly lost the acoustic connection to the device, which was re-established soon after. Furthermore, the position determination with the POSIDONIA system of the ship and the acoustic communication with the pressure sensor did not work simultaneously, probably due to the considerable water depth. After the device touched the seafloor we controlled the inclination, lifted it again 30 m and released it (14:00). During the hoisting of the deep-sea wire, two working measurement cycles were run, and then the data were uploaded with the acoustic modem.

After retrieving the deep-sea cable and acoustic modem, the air pulsers were installed again (19/03, 16:00). After we had traversed a long north-south profile with seismic refraction overnight, we stopped seismic operations at 10:20 am on 20 March. Immediately afterward, we started dismantling OBS/OBH instruments of the 3D experiment (Fig.5.5). Nine instruments remained on the seafloor for the final profile until the end of the seismic operations.

After recovering 13 instruments, we installed the third Chilean pressure sensor from IMO using the deep-sea cable at 08:00 on 21 March. Shortly after launching the device, we discovered that

the POSIDONIA acoustic locator was not working. After bringing the unit on deck and repairing a damaged connector, we deployed the pressure sensor again shortly afterward. The subsequent installation went smoothly, and by 13:00, the unit stood almost horizontal on the seafloor at 4454 m water depth and was working as expected. After retrieving the deep-sea wire, we continued retrieving the remaining OBS/OBH.

We dismantled 12 OBS/OBH stations overnight and installed five new instruments for the second profile (P100) of the cruise at noon on 22 March (Fig. 5.12). The subsequent dismantling of another eight stations went smoothly. At 23:00, we reached OBH 3D10, where we were able to measure the acoustic range but could not release the instrument. After many release attempts, we still located the OBH on the seabed and stopped recovering 3D10 for the time being. During the night, we recovered two more stations (3E09, 3D09) until 02:15 and then started a four-hour transit to the new profile P100 (Fig. 5.12).

On 23 March, we began the installation of 27 new OBS/OBH stations from east to west along profile P100 (Fig. 5.12). Around noon we interrupted the station deployment for 3 hours. During this time, a release test was carried out at 2000 m depth. Then, a floating test of a GEOMAR pressure sensor was carried out. The pressure sensor frame is based on an OBS frame modified during the current cruise (Fig. 11.6). Lastly, the MCS streamer (Fig. 11.2) was briefly lowered into the water for a functional test.

Profile P100 was completely installed at 02:00 on 24th March, and we continued with multibeam mapping until 08:00, which revealed some small seamounts and a complex structure of intersecting graben structures. At 08:00 on 25 March, the air pulsers and MCS streamer were deployed again, and FS SONNE started to acquire refraction data along profile P100 and towards the east. At the western end of the profile, the ship turned west to record ~30 miles of MCS data. Since the morning of 26 March, the dismantling of OBS/OBH along profile P1, starting with P134, commenced, and FS SONNE headed west.

On 27 March, we started the week with the acquisition of MCS data along profile P1. At 08:00, the streamer and air guns were hauled in to recover the first stations of profile P1. We started in the west with OBS P134 and were able to release and recover the OBS/OBH by the morning of 28 March without any major problems. Between station recoveries, we mapped smaller areas near the profile, such as a seamount of the Taltal Ridge, the top of which is only 630 meters below sea level and rises about 2500 meters above the surrounding seafloor (Fig. 5.1). Along the profile, eight OBS/OBH remained to the east. We deployed two additional OBS on the western side of the profile to obtain a small array of 5 OBS/OBH for an anisotropy experiment (blue circles in map, Fig. 5.5). To measure anisotropy, the air guns were deployed on the starboard side (28 March 2023, 10:20 am) to sweep three circles of 3, 5, and 8 nautical miles radius around the OBS stations by 29 March 13:00 (Fig. 5.5). Following this experiment, the 5 OBH/OBS were recovered. On the night of March 30, we headed east again to dismantle the remaining 8 stations on profile P100 and mapped a new area overnight with multibeam. The dismantling of the remaining stations went smoothly and finished at 17:00.

On the night of March 31, we visited the three Chilean pressure sensors along latitude 24.8°S (Fig. 11.5) to verify their operation. After deflecting an acoustic modem to 60 m water depth and the data and status of the device were read from the seafloor. We were able to read data from all three of the IMO's pressure sensors from the seafloor, and during the past week, all devices functioned as designed.

On 31 March and 1 April, the two pressure sensors from GEOMAR were installed during the daylight at 5400 m and 4650 m water depth, respectively. As with the IMO stations, a pressure sensor from Sonardyne is used. This was mounted on a modified GEOMAR OBS frame with a concrete anchor (Fig. 11.6). However, at the first station, we first encountered a strongly dipping seafloor, and the inclinometer showed a tilt of 22°. The instrument was then hoisted 50 meters and moved 150 meters to the north by ship. One hour later, the instrument was horizontal and fully functional on the seafloor.

On the evening of 01 April 2023, we went to the deployment position of OBH 3D10, which had responded but not released during the dismantling of the 3D experiment on 22 March. The station has an automatic time release. This was set for 02 April at 04:30 UTC, or 00:30 shipboard time. Overnight we were able to triangulate the position of the OBH acoustically at ~1900 m water depth very precisely, but it did not automatically ascend with the time release, nor did it respond to our release signals. On 2 April 2023, we were trying to recover the OBH 3D10 from the seafloor by dredging. For this purpose, the deep-sea cable (>7,500 m) was laid out in a circle around the station with a radius of three cables (~555 m) and then slowly tightened so that the hooks could catch the station and hoist it onto the deck. Unfortunately, the dredge seemed to have missed the OBH, so we left the site in the afternoon in the direction to the west and commenced multibeam until the border of the working region. We left the working region at 23:59 on 04 April 2023 and constantly moved towards the northwest to Guayaquil. The transit was interrupted on 09 April because the Peruvian coastguard asked RV SONNE to check a closeby coordinate (~20 nm) where a fishing vessel reported its last position on 8 March 2023. Arrived at the given position, we just found other fishing vessels, some wood and a plastic box of unknown origin on the water. We continued heading towards Guayaquil and RV SONNE reached the entrance of the Río Guayas on April 11, 2023, at 04:00. After travelling the river upwards for 50 km, RV SONNE reached the harbour of Guayaquil in the same morning at 09:00, terminating cruise SO297.

5 Preliminary Results

5.1 Hydroacoustics (Multibeam Bathymetry, Backscatter and Parasound)

(I. Klaucke[1], M. Riedel[1] and watchkeepers)
[1]GEOMAR

5.1.1 System parameters

The Kongsberg Simard EM122 of RV SONNE operating at 12 kHz has a 0.5°x1.0° beam width, and was used throughout cruise SO297 in order to record bathymetric, backscatter and water column data. High-density equidistant and chirp (FM pulse) multi-ping mode with the FM (chirp modulated) pulse and a reduced swath width of 130° total swath were set for high soundings density and quality to the detriment of coverage. These settings produce 864 soundings per ping. A total of four sound velocity profiles were acquired using a Seabird CTD. Data quality was good considering ideal sea state conditions with few wind waves and only long wavelength swell.

However, many drop-outs in the near nadir region and some consistently erroneous depth values for portions of the swath are unusual for this system and have been attributed to biofouling on the transducers. Besides travel times, the signal amplitude of the multibeam echosounder is stored by the acquisition software SIS. Some preprocessing, including altitude processing as well as time and angle varying gain, is applied to the data prior to storage.

The Teledyne-Reson P70 PARASOUND echosounder installed onboard RV SONNE operates based on the parametric effect of the nonlinear relation of pressure and density during acoustic wave propagation. Two acoustic waves with frequencies of 18-20 kHz (primary high frequency, PHF) and 22-24 kHz are emitted, creating a secondary high (40-44 kHz, SHF) and a corresponding secondary low (2-6 kHz, SLF) frequency wave. The SLF is used for the sub bottom profiling and sediment imaging; the PHF can instead be used for imaging of gas bubbles, plankton or fish in the water column. During cruise SO297 18 and 22 kHz primary frequencies have been used for ~4 kHz SLF. In total more than 4000 line-km of PARASOUND data were acquired continuously along profiles or transits between stations, but not while the vessel was stationary (e.g. during OBS recovery).

5.1.2 Preliminary results

A total of about 38,000 km² (which, for comparison corresponds to slightly less than the Coquimbo region in Chile or slightly more than Baden-Württemberg) were mapped during the cruise covering two extended areas around Taltal Ridge (Fig. 5.1) and Copiapó Ridge (Fig. 5.2), as well as a transit line between the ridges. Data processing has been carried out onboard using Caraibes 5.0 for bathymetry and FMGT for backscatter data. Bathymetry processing included triangulation filtering and manual editing of erroneous soundings. Valid soundings were then exported and gridded with the Generic Mapping Tool (GMT) using a nearneighbor algorithm that required one sector out of four to be filled, and a search radius (60 m) slightly larger than the grid cell size (50 m), allowing for some interpolation and smoothing. An additional grid with a 100 m grid cell size and 150 m search radius was also calculated. Water depths of up to 8000 m required several swaths covering the same area and a certain degree of oversampling in order to justify a 50 m grid cell size. The 50 m grid is probably at (or even beyond) the maximum resolution of the RV SONNE EM 122 system in such water depths.

The backscatter data were crudely processed on board applying radiometric corrections, angle-varying gain and anti-aliasing filters in order to produce a georeferenced mosaic. However, the backscatter data require additional manual editing and turn elimination in order to improve the product. Bathymetric data, on the other hand, were fully processed during cruise SO297 and the data are available for post-cruise work. In total, a distance of ~4200 km of hydroacoustic data was acquired.

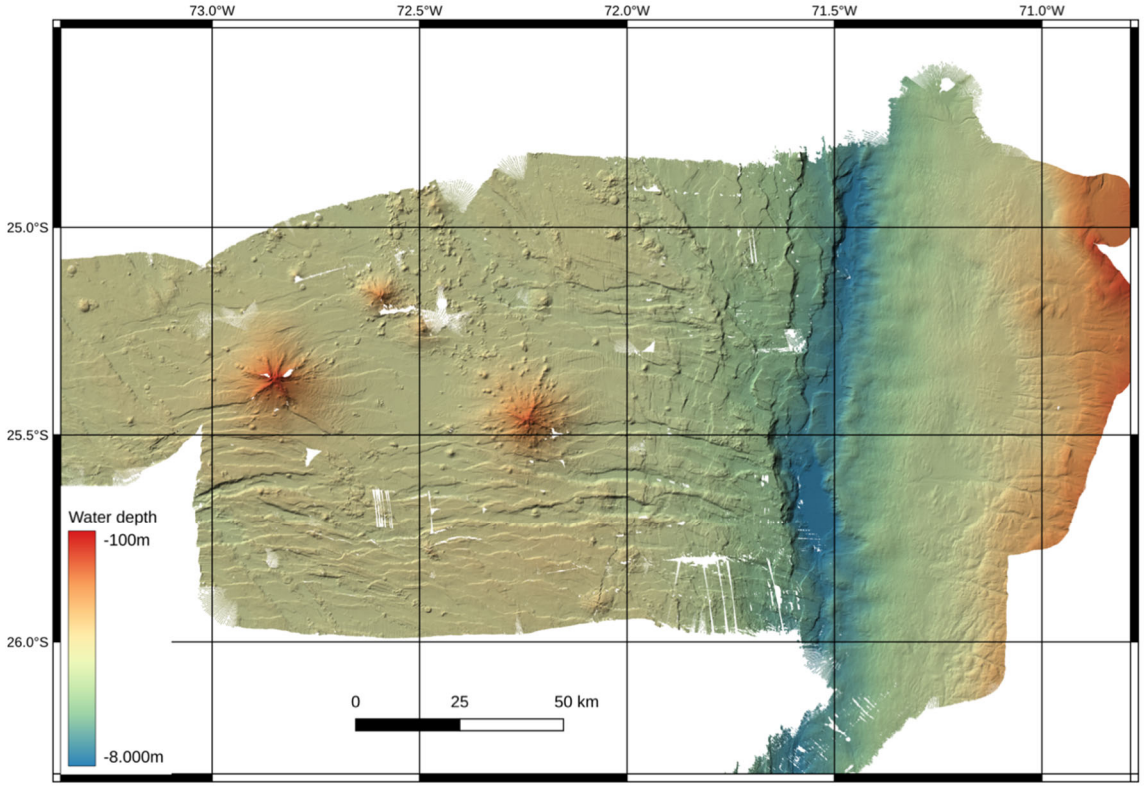

Fig. 5.1 Map of bathymetric data acquired during cruise SO297 over Taltal Ridge and the adjacent continental slope offshore Chile, showing several seamounts, a sediment-starved trench and W-E-trending horst-and-graben structures.

The newly mapped area offshore Taltal (Fig. 5.1) shows a relatively smooth lower continental slope and a series of canyons dissecting the upper slope. The upper slope also shows a certain degree of slope retreat between 25.2°S and 25.6°S. The trench reaches almost 8000 m of water depth and is mostly devoid of sediment, except for a small basin south of 25.5°S. Several smaller, cauliflower-shaped embayments on the lowermost slope probably hint towards past slope failures. The W-E-trending Taltal Ridge is characterized by large and tall (up to 3500 meters above the surrounding seafloor) seamounts that are surrounded by an area with W-E-trending horst-and-graben structures that are quite unexpected in this location. The throw on the bounding faults reaches up to 500 metres. Similar structures have not been found further south along Copiapó Ridge, which is located around 27°30'S (Fig. 5.2). Copiapó Ridge shows a series of seamounts that become affected by N-S-trending bend faults when approaching the trench with some possible reactivation of faults that show an NW-SE orientation (i.e. Copayapu-I, Fig. 5.2). This latter orientation is believed to represent the spreading fabric of the oceanic plate, and is quite prominent in most areas unaffected by seamounts.

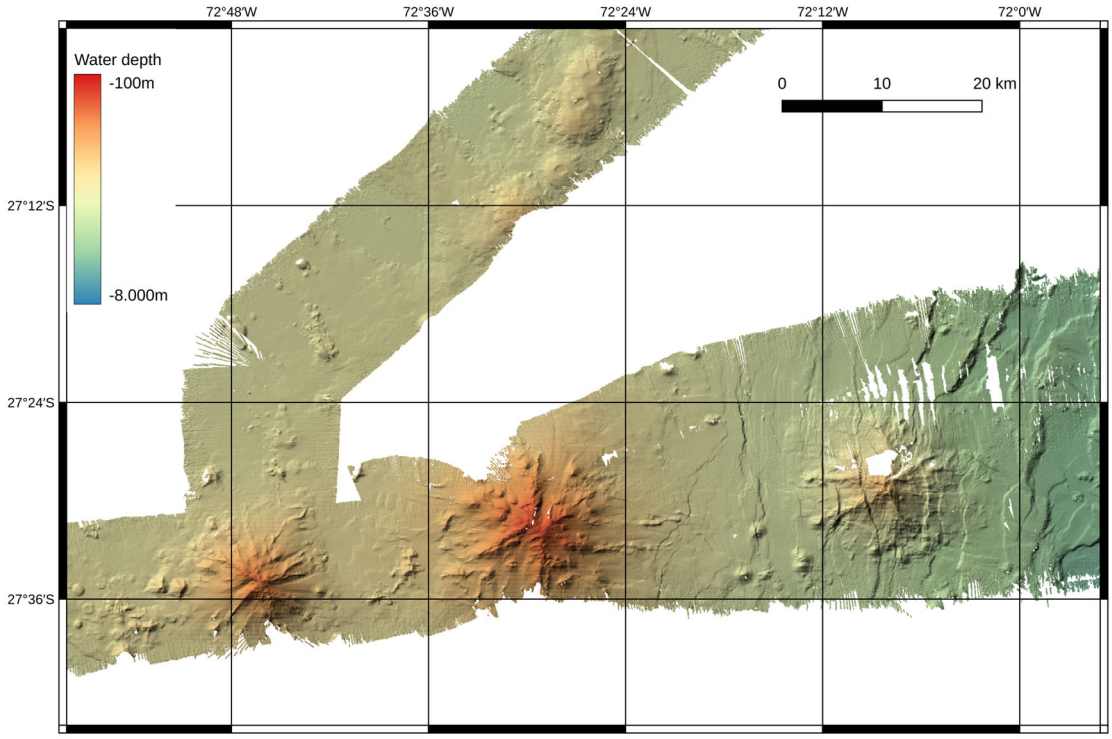

Fig. 5.2 Bathymetric map of three seamounts (from East to West Copayapu-I, II and III) based on data acquired during cruise SO297.

5.2 Seafloor Geodesy with Absolute Pressure Sensors

(M. Moreno[1], J. Diaz[2])
[1] Universidad de Concepción, [2]Pontificia Universidad Católica de Valparaíso

The larger earthquakes and the most destructive tsunamigenic earthquakes occur underwater, a location where few direct measurements of earthquake-related deformation are available worldwide. Such offshore data can provide new constraints needed to estimate slip and associated seismic and tsunamigenic hazards all the way to the trench, complementing existing geodetic and seismic networks on land. In particular, ocean bottom pressure sensors with the new ability to remove instrumental drift are novel tool for determining vertical seafloor displacements with millimeter to centimeter resolution, critical observations for better understanding earthquakes and slow slip events (SSE).

The FONDEQUIP Integrated Deep-Ocean Observing System (IDOOS) project, funded by the National Agency for Research and Development (ANID), together with GEOMAR (Kiel, Germany), carried out the installation of five pressure sensors during the SO297 cruise. Three of these sensors are part of the IDOOS project led by the Millennium Institute of Oceanography (IMO), and two are from GEOMAR, Kiel. This joint Chilean-German project aims to provide an in-depth understanding of the slip behavior of the shallower segment of the seismogenic zone of large earthquakes in Chile and to delineate the updip extension of the locked zone, its structure and mechanical control, and key information for seismic hazard assessment. Hence, this is a cutting-edge, high-risk, high-reward research project that pursues highly innovative and technological research with the potential for broad impact and high societal impact for Chile.
Seafloor pressure sensors can detect vertical changes in the elevation of the sea floor. However, seafloor pressure data include contributions from a variety of sources and may not provide the accuracy required for geodetic investigations on their own. There are two main challenges in using bottom pressure gauges for seafloor geodesy (Wilcock et al., 2021): 1) correcting pressure observations by removing oceanographic signals; 2) correcting for the tendency of pressure sensors to drift (Wilcock et al., 2018).

Seafloor pressure variations are influenced by tidal and regional or mesoscale atmospheric/oceanographic changes. To remove oceanographic noise from the observed seafloor pressure time series, oceanographic measurements of conductivity, temperature and pressure (CTD) at different water depths and an ocean circulation model are needed. As part of the IDOOS project, in September 2023, we will be installing two deep ocean moorings near the pressure sensors with several oceanographic instruments that will allow us to correct for oceanographic noise. Seafloor pressure sensors have an inherent drift, which cannot be predicted from laboratory calibrations. The five pressure sensors installed during the Cruise SO297 are Sonardyne 8306 Fetch Ambient-Zero-Ambient (AZA) Transponders.

The AZA method is a technique that allows long-term sensor drift in a high-range pressure sensor to be measured periodically in situ. The AZA option permits the quartz pressure sensor to be recalibrated in situ by periodically taking it to one atmosphere and measuring the sensor bias against a low-pressure sensor of similar quality. A valve is used to periodically switch, for a short time, the measured pressure from the external ocean to the inside of the instrument housing at atmospheric pressure. The internal pressure reading is compared to an accurate barometer to measure the drift, which is assumed to be the same at low and high pressures. This self-calibrating

pressure recorder can reduce instrument drift to about 1 millimeter (1 ppm of full scale) per year (Wilcock et al., 2021), efficiently eliminating drift to enable long-term measurements of geodesy and sea level change. The resulting drift-free pressure record can be used to obtain vertical seafloor motion better than 0.4 cm/yr. These geodetic sensors also include high-precision tiltmeters, which are useful for estimating the direction of seafloor deformation. They also have temperature sensors (Fig. 3.2.3) that will allow us to monitor the temperature of the ocean at great depths.

The pressure sensors are mounted on tripods that allow them to be placed in a stable position on the seafloor. These sensors have to be installed in an area with less than 10º slope. The installation was done by means of a cable that allows very precise positioning of the sensors. Fetch is a long-life subsea sensor logging node that enables wireless data extraction via its integrated high-speed acoustic modem. The sensors are powered by a 5-year lithium battery with excellent corrosion resistance. We plan to make annual visits to download data and check instrument performance. The three IDOOS sensors are expected to operate for five years, while the two GEOMAR sensors are expected to operate for two to three years.

Figure 5.3 shows data examples of the data uploaded from the seafloor after approximately 10 days after installation. Station PRS3 started to tilt after 7 days of installation, likely related to water currents close to the seafloor.

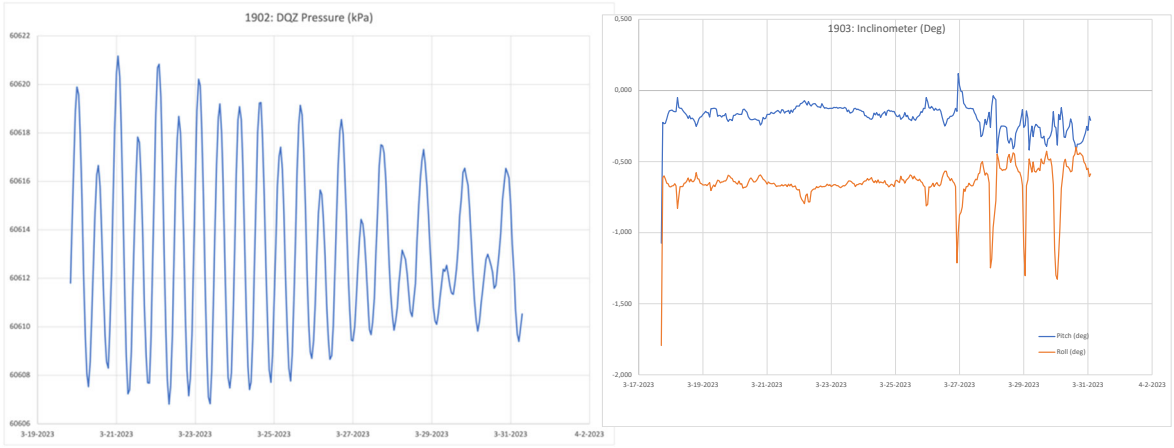

Fig. 5.3 Plot of the pressure from PRS3 (left panel) and inclination (right panel) recorded by the PRS1 from March 17 to March 31, 2023. The peaks emerging on 27 March are likely related to tidal currents.

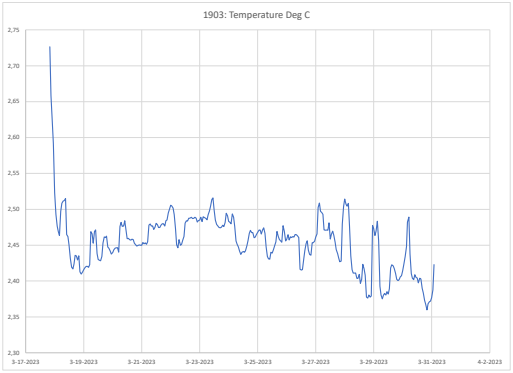

Fig. 5.4 Plot of the temperature recorded by the PS01 sensor from the 17th to the 31st of March 2023.

5.3 Seismic Survey

(A. Dannowski[1], A., M. Kühn[1], E. Contreras-Reyes[2] and watchkeepers)
[1]GEOMAR, [2]Universidad de Chile

High resolution 2D and 3D seismic data were acquired in order to image subsurface structures and sediment coverage across the North-Central Chile Subduction Zone, covering ~2440 km profile length (Figs. 5.5 and 5.6) recorded on 114 OBS and OBH sites. Two OBH could not be recovered. In total, we shot ten seismic surveys with different acquisition geometries (Fig. 5.3.3 until 5.3.8). A majority of the surveys were designed to optimize refraction seismic experiments with a shot interval of 60 seconds. The streamer system was active during these surveys (except for parts of P6000 and P7000 due to technical problems with the streamer system). Specifically, multichannel reflection seismic (MCS) data were acquired along two west-east trending profiles in the 3D array at a shot rate of 18 s. After completing the seismic profiles and the 3D array, a seismic anisotropy survey was shot without the streamer system.

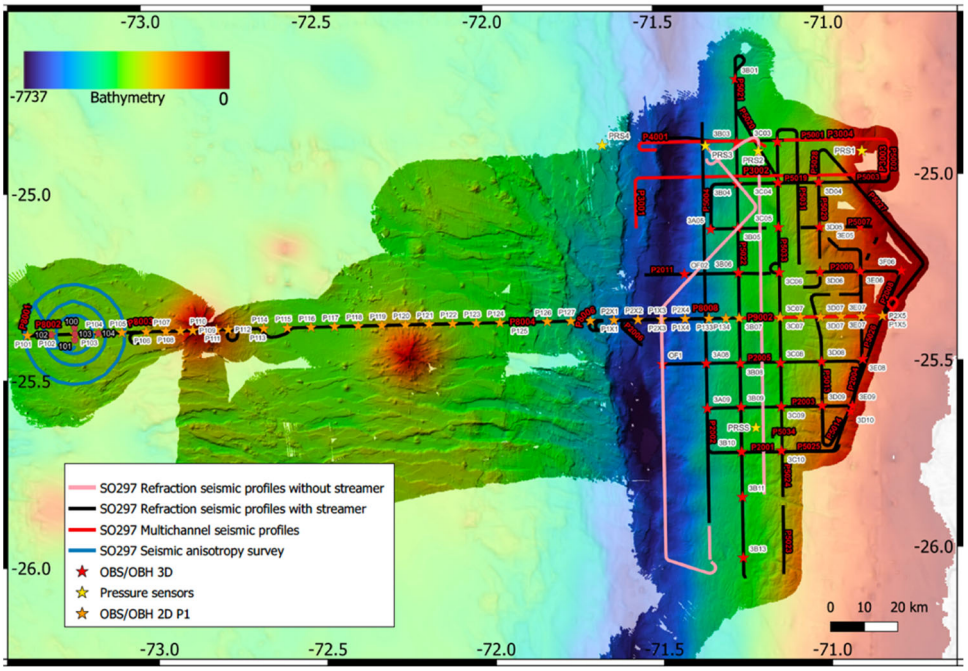

Fig. 5.5 Overview map of the seismic profiles acquired during SO297 (northern survey area). The survey P6000 (except P6001) and the P7000 were shot without the streamer system.

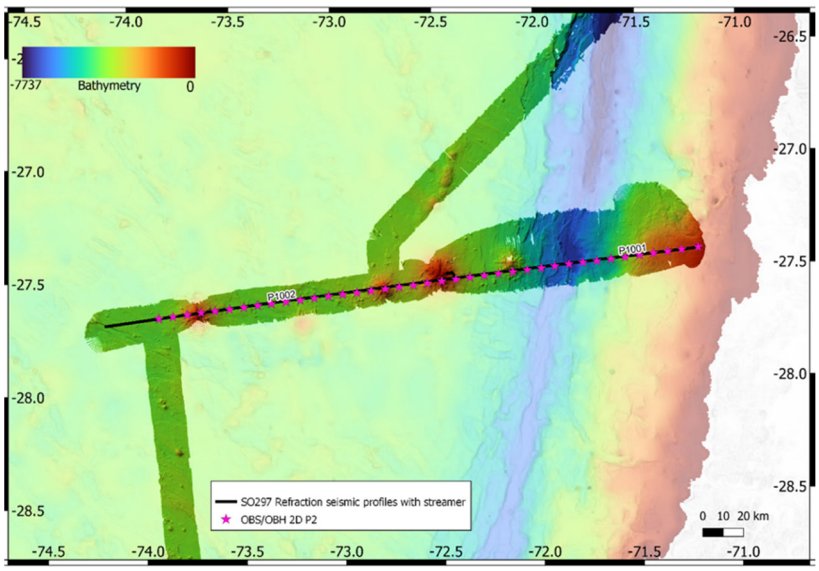

Fig. 5.6 Overview map of the seismic profile P200 acquired during SO297 in the southern survey area.

5.3.1 Seismic source

5.3.1.1 G-Guns

A G-Gun array produced by Sercel Marine Sources Division and Seismograph Services Inc. was used as source during the data acquisition of the seismic surveys. The array consists of 12 guns, which were set up at starboard and port side of the ship in 3 clusters each. 2x8 litre G-Guns were placed at the outer positions that framed either 2x4 litre or 2x6 litre G-Guns, which were placed in the inner positions. This gun distribution was chosen because it provides a good primary-to-bubble signal ratio, and the total volume of the six guns amounts to 37.6 litres, which should enable significant penetration. Airgun-deployment rails mounted on RV SONNE were used to deploy the G-Gun array. During data acquisition, the array was towed 40 m (shot point centre 44 m) behind the ship's stern. The guns are towed 8 m below the sea surface and triggered at a pressure of 140-145 bar. In order to achieve maximum ray coverage, the G-Gun array was used with a shot interval of 60 s, which roughly translates to a shot point distance of 120 m at 4 kn speed during the seismic refraction experiment. Similar to the receiver distance, the shot interval was chosen to optimize the prerequisites for a later velocity inversion.

For the dedicated multichannel seismic imaging experiments (P3000, P4000, P9000), only one side of the array was used for one shot and the shot time interval was shortened (see Tab. 1) to increase the trace coverage ("fold") in the MCS profiles.

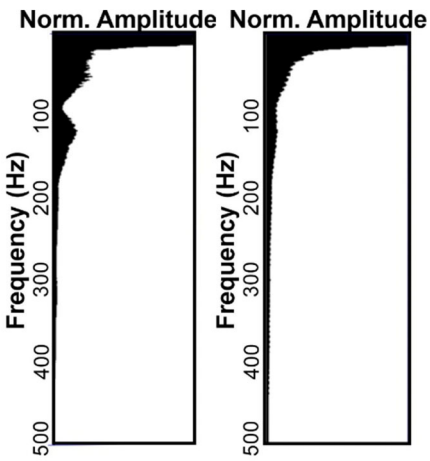

Fig. 5.7 Amplitude spectra from two different surveys. Left: Shot spectra of ten shots stacked from survey P2000. Right: Shot spectra of ten shots stacked from survey P9000.

5.3.1.2 Gun GPS and tuning

Knowing the exact experiment setup is a crucial part of data processing and analysis of high-resolution seismic data. A GPS situated directly on the airgun

delivers this part of information since the shot position at the shot time will exactly be known independent of the side drift of the array in the water caused by wind, water currents or during profile turns. A new generation of Airgun GPS was tested and further developed during the shooting of all seismic lines. This allowed us to perform an anisotropy experiment, shooting in cycles around the deployed stations.

To enhance the signal-noise-ratio and transmit more energy into the seafloor, a directed source can help. For this reason, the last 20 shots of profile P5022 and the first 80 shots of line P100 were used for airgun tuning tests. The G-Gun clusters were shot with a delay of 1.6 ms between the cluster closest to the vessel and the one furthest away, resulting in a delay of 0.8 ms between each cluster, parallel on both sides of the array.

5.3.2 Multichannel Streamer Seismic Profiling

5.3.2.1 Streamer setup

We used 7 to 8 active sections (Geometrics GeoEel streamer segments, each 12.5 m long) with an overall digital streamer length of 87.5 m to 100 m for recording the seismic signal. Deck geometries, streamer configuration and seismic gun settings for the 2D survey are illustrated in Figs. 5.8. The seismic recording unit consists of a 50 m long tow cable and the active sections attached behind the tow cable. Each active section contained eight hydrophones with a group spacing of 1.56 m. Each active streamer section had an analog-to-digital (AD) converter module. Communication between the AD digitizer modules and the recording system in the lab was transmitted via TCP/IP protocol. A repeater was located between the deck and tow cables (Lead-In). The streamer power supply unit managed the power supply and communication between the recording system and the AD digitizer modules. A small buoy was attached to the tail swivel of the 2D streamer. Starting with P2000, a weight with a 20 m line was placed between the tail swivel of the streamer and the tail buoy to increase the stability of the system in the water and reduce flow-noise induced by the tail-buoy.

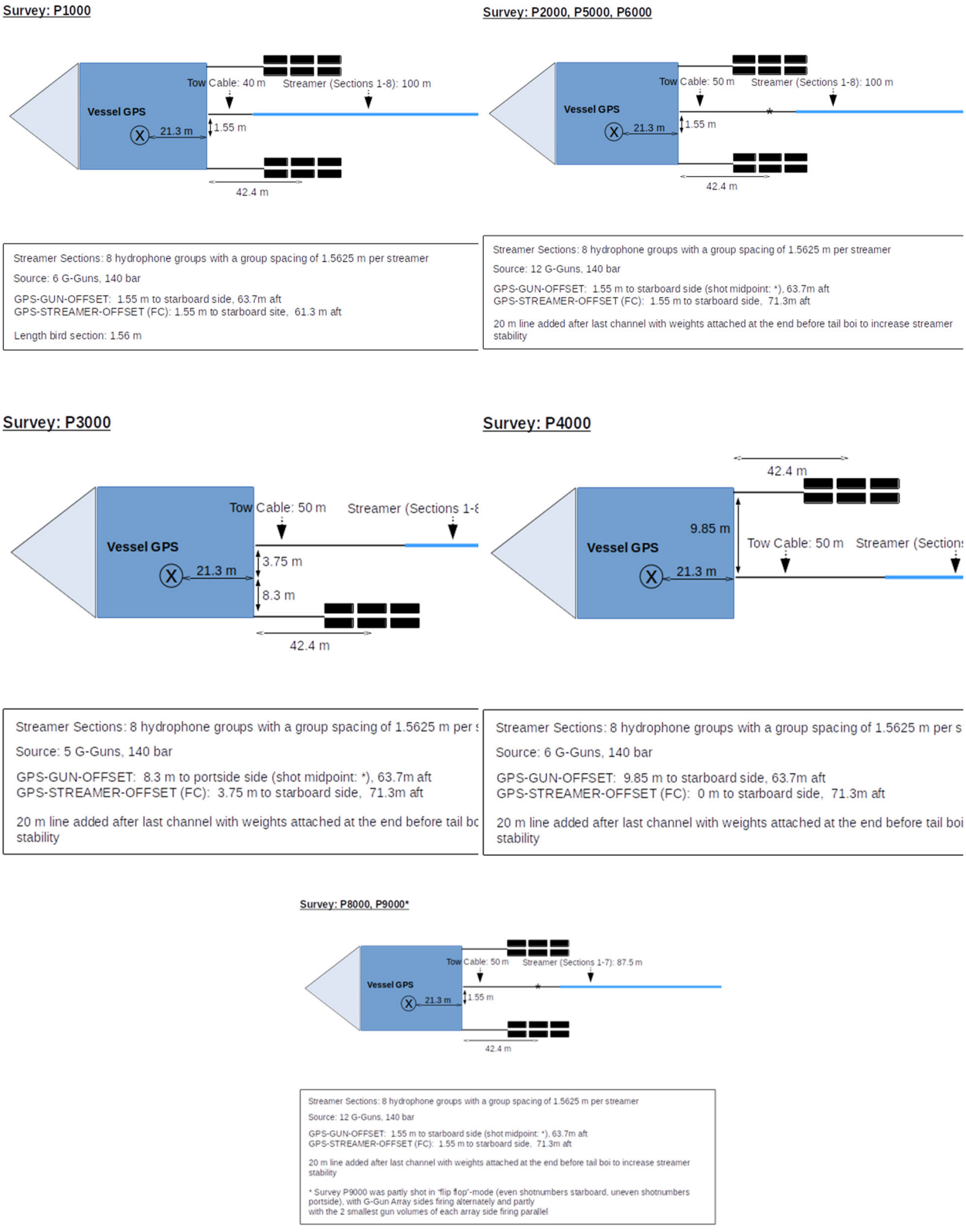

Figures 5.8 Deck geometry for survey the different surveys.

5.3.2.2 Data Recording and Processing

Data were recorded with acquisition software provided by Geometrics. The analogue signal was digitized with a sample rate of 1 millisecond. The seismic data were recorded as multiplexed SEG-D. One file with all channels within the streamer configuration was generated per shot. The corresponding logged shot file reports the shot number and time information contained in an RMC string. The acquisition PC allowed online quality control by displaying shot gathers, a noise window, and the frequency spectrum of each shot. The cycle time of the shots was displayed as well. The vessel's position was simultaneously logged in the RMC string along with logged time and position information with a GPS antenna. On-board processing included streamer geometry configuration, delay calculations and source and receiver depth control. From the seismic data a delay of -50 ms was defined.

The source-receiver locations were then binned with a common-midpoint spacing of 6.25 m (P1000, P2000, P5000, P6000, P8000) or 3.125 m (P3000, P4000, P9000). Different filter tests were performed and the frequency spectra (Fig. 5.9) were analyzed. Seismic traces were balanced and filtered using a bandpass filter with corner frequencies at 5, 15, 350, 450 Hz (P1000 to P8000) or 15, 35, 350, 450 Hz (P9000, Fig. 5.9). Subsequently, common-midpoint sorting, a normal move out correction (with a constant velocity of 1510.00 m/s, derived from a CTD measurement), stacking and exponential gain (exp= 1) were applied. The stack was migrated with a 2D Stolt migration algorithm using a constant velocity model of 1500 m/s.

Tab. 5.1 Source and receiver parameters during the different seismic surveys during SO297.

Profile	Shotrate [s]	Record length [s]	Trigger/shot-delay [ms]	No. of channels	Pressure [bar]	No. of air guns	Total gun volume [cu]	Source depth [m]	Receiver depth [m]
P1000	60	16	50	64	140 - 145	12	5420	8	2-4
P2000	60	16	50	64	140 - 145	12	5420	8	2-4
P3000	18	16	50	64	140 - 145	6	2840	8	2-4
P4000	18	16	50	64	140 - 145	6	2580	8	2-4
P5000	60	16	50	64	140 - 145	12	5420	8	2-4
P6000	60	16	50	64	140 - 145	12	5420	8	2-4
P7000	60	16	50	-	140 - 145	12	5420	8	-
P8000	60	16	50	56	140 - 145	12	5420	8	2-4
P9000	10 -12	9	50	56	140 - 145	4-6	1260 - 2840	8	2-4
Anisotropy Survey	30	-	50	-	140 - 145	6	2580	8	-

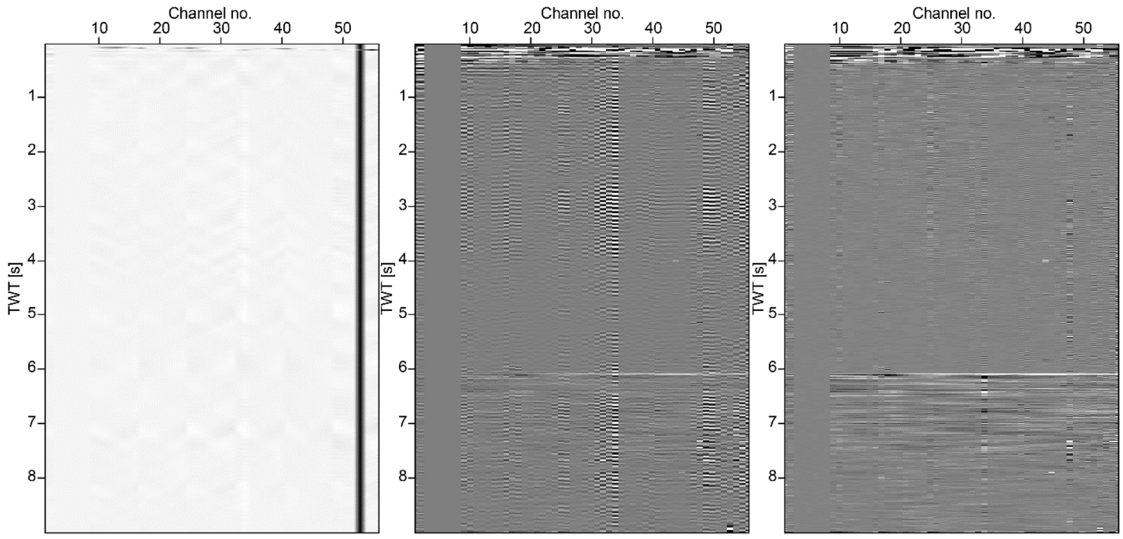

Fig. 5.9 Filter test procedure for one shot from survey P9000. Right: unfiltered shot. Low frequent noise is dominant, no primary reflections are visible. Middle: bandpass filtered shot (5, 15, 350, 450 Hz), reflections become visible at 6 s TWT. Signal-to-noise-ratio is still poor. Right: bandpass filtered shot (15, 35, 350, 450 Hz). Signal-to-noise-ratio is significantly increased. Note that channels 3 to 8 did not record data throughout all surveys.

5.3.3 Refraction Seismic Profiling

At 115 locations GEOMAR's short-period Ocean Bottom Seismometer (OBS) and Ocean Bottom Hydrophones (OBH) were deployed in three different survey areas: along profiles p100 with 41 stations and p200 with 39 stations; 33 OBS/H in a 3D array and two additional instruments at the western end of p100 to support a study about the anisotropy of the oceanic crust. The source is described in section 5.3.1. Instruments, data quality and first results are described in the following.

5.3.3.1 Ocean Bottom Seismometer

Four types of OBS were deployed, each carrying different types of pressure tubes. Ten instruments were of the type OBS-2002, while six of these had round flotations. The other four OBS had flotations in cube shape. This results in different drifting behaviors during the free fall to the sea floor. The other main type of OBS was the Lobster design, where six 8000-m OBS with round flotations were used. The remaining Lobster instruments had cube-shaped flotations with a depth limit of 6000 m water depths for the flotations and the pressure housings.

The OBS-2000 design was based on experiences gained by the work with the GEOMAR Ocean Bottom Hydrophone (OBH; Flueh and Bialas 1996) and the GEOMAR Ocean Bottom Seismometer (OBS, Bialas and Flueh, 1999). Tthe Lobster design is a further development of K.U.M GmbH based on the work with the OBS-2000 design.

The used OBS systems record the emitted seismic wavefield by measuring both the acoustic pressure in the water column and the local ground displacement, which are measured by a mounted hydrophone of the type HTI-01-PCA, and HTI-90-U (High Tech Inc.) or an OAS hydrophone and a 4.5 Hz three-component seismometer (K.U.M, modified after Tim Owen (Cambridge)).

Three types of pressure tubes were used that were the housing for the recording units: standard pressure tube that protects the gear from substantial pressure down to 6000 m water depth and a larger and heavier pressure tube resisting 8000 m water depth (both types can host a GEOLOG or a Sercel recorder); KUM 6D6 pressure tube that can host the 6D6 recorder (both, tubes and

recorders were rented from Bundesanstalt für Geowissenschaften und Rohstoffe, BGR). All tubes and housings are produced from titanium to resist the given environmental conditions in the deep sea. The entire system weight is ~180 kg for the OBS-2000 design and ~250 kg for the Lobster design, including the anchor weight for the instrument drop.

The OBS possesses a flotation body of synthetic foam, producing enough buoyancy to hold the OBS at the sea surface. Syntactic foams are composite materials synthesized by filling a metal, polymer, or ceramic matrix with hollow spheres called micro balloons or cenospheres or non-hollow spheres (e.g. perlite). The buoyancy of the OBS is counteracted by a massive anchor frame (~60 kg), which is attached horizontally to the bottom of the OBS before deployment and is released when the OBS is to be retrieved. The release is made possible by an acoustic release transponder (the K/MT562;), which disconnects the OBS from the anchor frame, causing the OBS to rotate by 90° and start to ascend to the sea surface when a specific signal is emitted into the water column. The rotation of the OBS during its ascend is caused by the position of the instrument's centre of mass and results in the transponder unit of the OBS remaining underwater and thus being able to react to emitted range signals enabling its localisation.

5.3.3.2 Ocean Bottom Hydrophones

The first GEOMAR Ocean Bottom Hydrophone was built in 1991 and tested at sea in January 1992. This type of instrument has proved to be highly reliable; there have been more than 7000 successful deployments since 1991. Because of the age of the instruments, locations were chosen to a maximum water depth of 4000 m.

The principle design and a photograph of the instrument during deployment are shown in Fig. 5.10. The design is described in detail by Flueh and Bialas (1996).

The system components are mounted on a steel tube, which holds the buoyancy body on its top. The buoyancy body is made of syntactic foam and is rated, as are all other system components, for a water depth of 6000 m. Attached to the buoyant body are a radio beacon, a flashlight, a flag and a swimming line for retrieving from aboard the vessel. The hydrophone for the acoustic release is also mounted here. The release transponder is produced by OCEANO Technologies or iXBlue. Communication with the instrument is possible through the ship's transducer system, and ranges of 3 to 4 miles release and range commands are successful. For anchors, we use pieces of railway tracks weighing about 40 kg each. The anchors are suspended 1 m to 2 m below the instrument. The sensor is an HTI-04-PCA or an HTI-90-U hydrophone from High Tech Inc. The recording device is a GEOLOG recorder or a Sercel recorder, contained in its own pressure tube and mounted below the buoyant body opposite the release transponder (see Fig. 5.10).

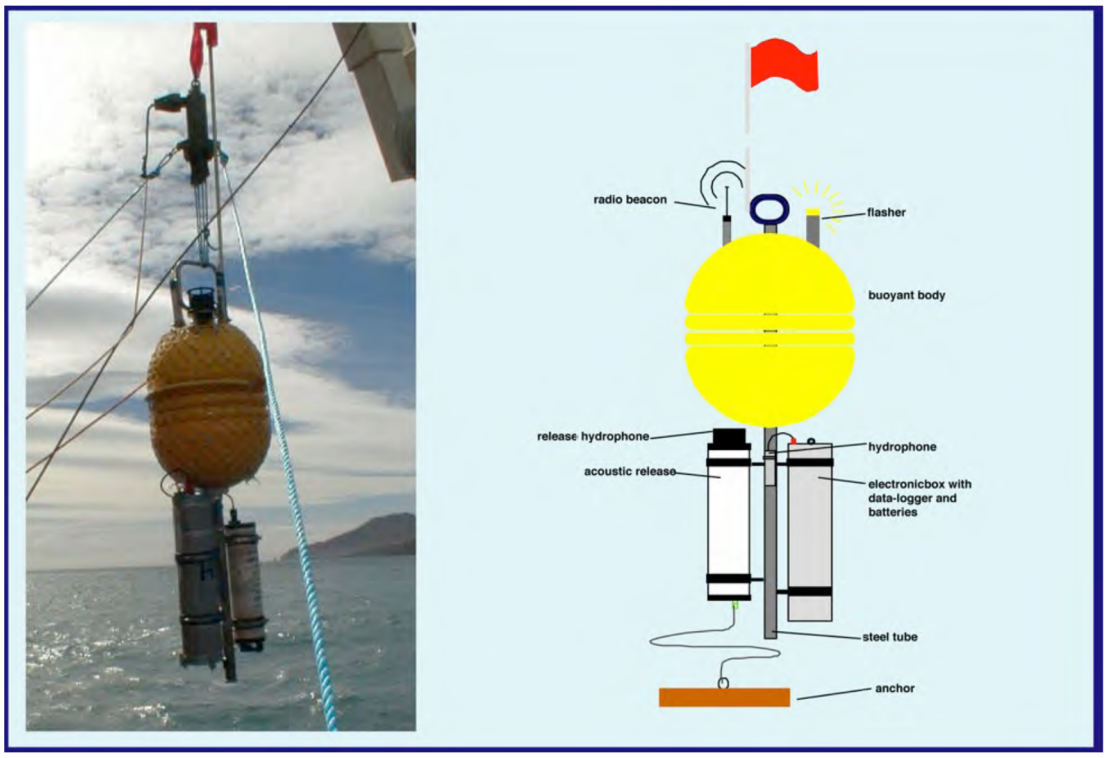

Fig. 5.10 Photo and sketch of the GEOMAR OBH (right panel, after Flueh and Bialas, 1996) and the instrument upon deployment (left panel).

5.3.3.2 OBS data acquisition

All recorders measured data with a sampling rate of 250 Hz, independent of the type of recorder. Three different types of recorders were used: GEOLOG recorders, developed at GEOMAR, Sercel recorders, developed at/for Ifremer and 6D6 recorders, developed by K.U.M. GmbH. The recorder is fed by an external power source and has a precise clock to record seismic data with high accuracy. The recorder and the power source are encased in titanium tubes, as described above. An autonomous time signal needs to be generated. The clock of the recorder is synchronized shortly before deployment using a GPS time signal. After instrument recovery, the clock will be synchronized a second time to determine the clock drift of the recorder's clock. This drift will be corrected when cutting the continuous data into SEY-shot-sections. As onboard pre-processing of the data, filtering and deconvolution with standard values have been applied to the data for a first quality check (as presented here). More detailed processing is required for further in-depth analysis.

5.3.4 Preliminary results

5.3.4.1 MCS

Overall, the seismic imaging capacity using the short streamer with offsets < 200 m is limited due to the low fold from large shot-point spacing. Here, we show one example of profile P9002 consisting of an MCS line shot with faster shot-point interval (Fig. 5.11). The imaging shows low depth-penetration of mostly < 0.5 s two-way time (equivalent to < 400 m depth). A series of normal faults can be identified on the upper slope between CDP 1000 and 5000. These are linked to sediment-filled mini-basins on the down-slope side of the fault traces. The easternmost two faults

are seen as clear offsets in the basement but have no associated change in seafloor topography. In contrast, the westernmost two faults are linked to clear steps in seafloor bathymetry. In total, approximately 2.151 km MCS data was acquired.

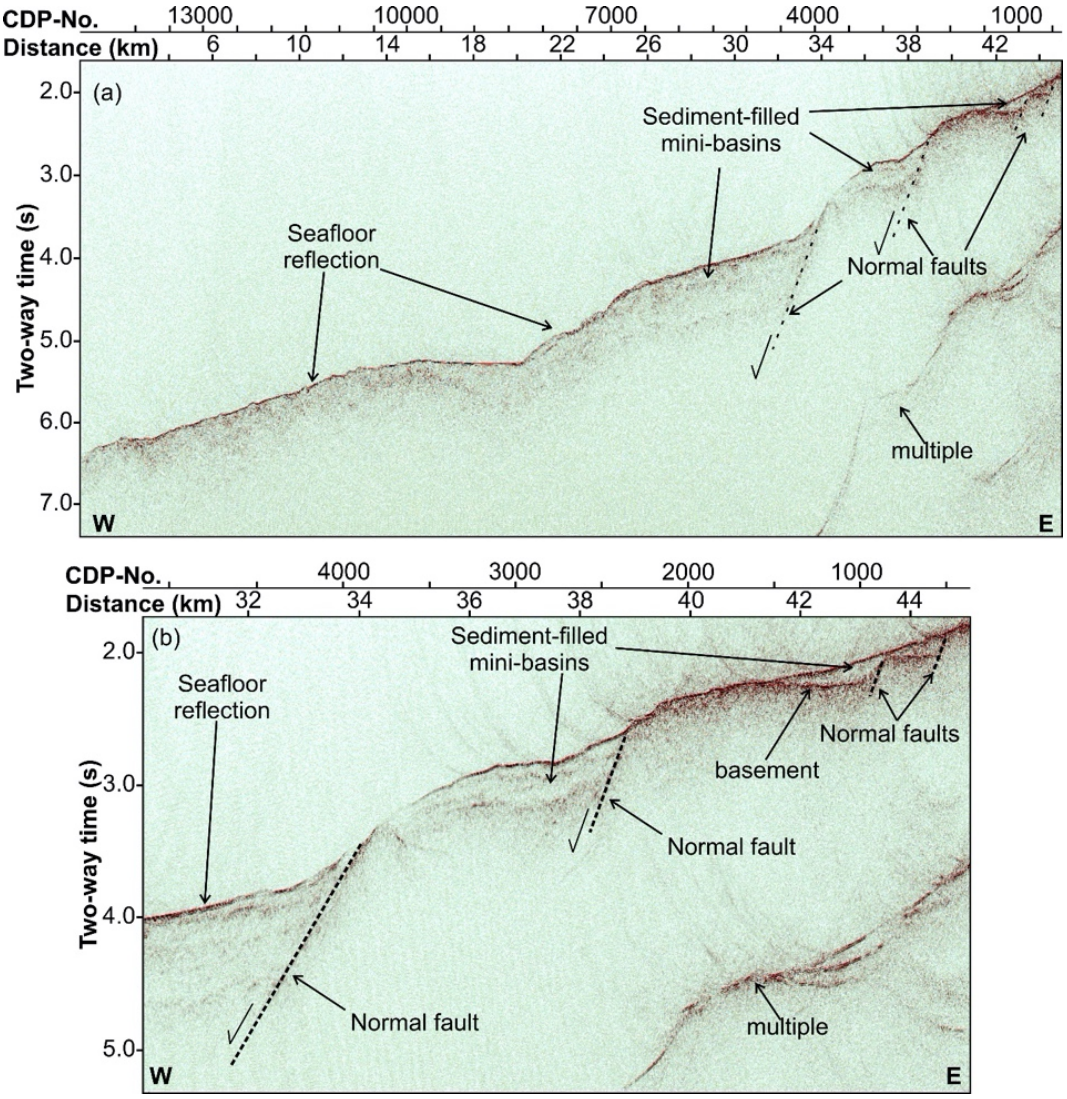

Fig. 5.11 (a) Image of MCS line P9002 (location see Fig. 5.3.1) with preliminary interpretation. (b) On the upper slope portion of the profile between CDP 1000-5000, several normal faults are seen, indicative of extensional deformation related to processes of the sub.

5.3.4.2 Profile P100

Seismic profile P100 is oriented parallel to the Taltal Ridge axis with a total length of approximately 248 km (Fig. 5.12). In total, 42 seismic stations were placed along the line at a spacing of 5 km except at the Taltal Seamount II (TTSII), where a denser spacing was used to increase the seismic resolution around this extinct volcano (Fig. 5.12a). Due to the presence of aquatic mammals, the airgun was stopped several times, causing short seismic gaps in the seismic records. However, the data quality is excellent with offsets of mantle refractions up to 140 km. Fig. 5.12b shows a seismic record example of OBS133.

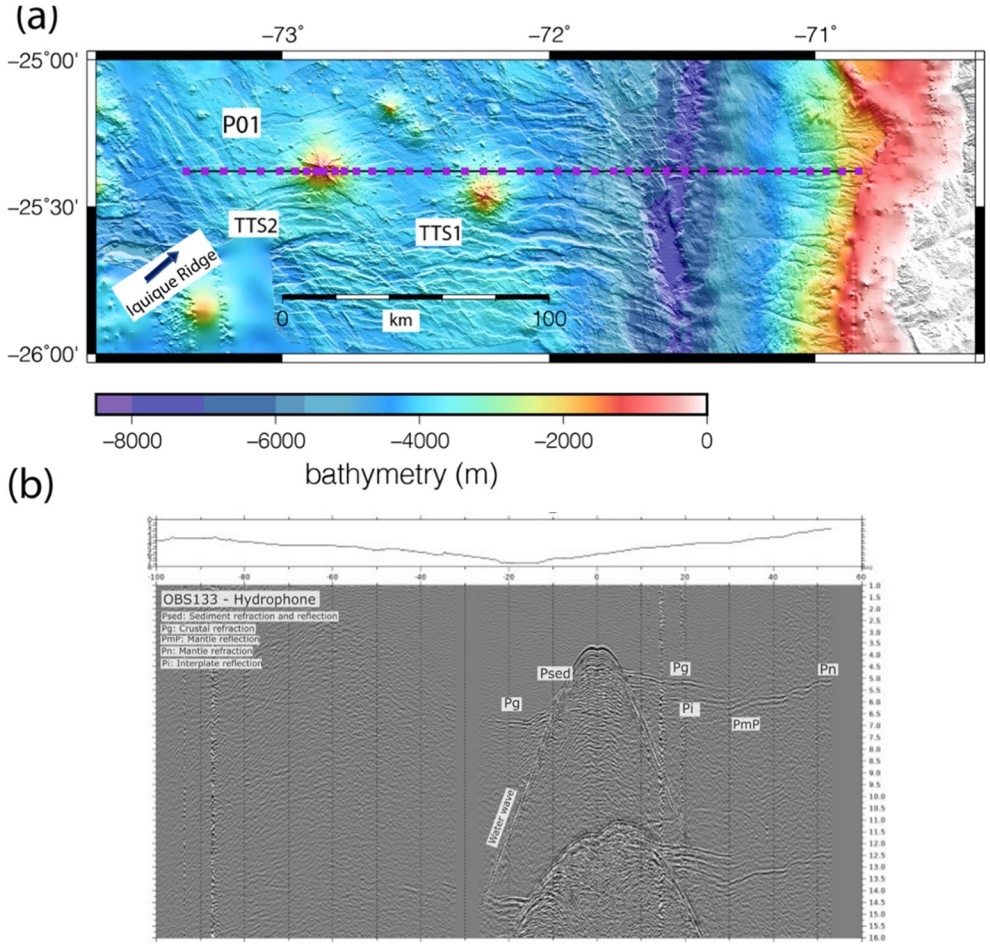

Fig. 5.12 (a) Swath bathymetric image of the seafloor off Taltal region. The Taltal seamounts I-II (TTSI and TTS2) correspond to the easternmost portion of the Taltal Ridge before the collision with the South American plate (Contreras-Reyes & Carrizo, 2011). Black line denotes the wide-angle seismic profile P100. Dots correspond to the deployed 42 OBH/S. (b) Hydrophone component of OBS133 situated on the forearc.

5.3.4.3 Profile P200

Seismic line P200 was approximately 295 km long and provided excellent seismic data from a line covering the incoming plate, the trench, the marine forearc and the Copiapó Ridge. A total of 39 OBS and OBH were deployed along the line (Fig. 5.13a). Unfortunately, one station could not be retrieved due to problems in the buoyancy system of the OBH. There is also a seismic gap near the Copapyapu Seamount IV due to the presence of marine mammals. However, crustal (Pg) and mantle (Pn) refractions, as well as Moho reflections (PmP), can be observed in the seismic records with high quality. Many stations placed in the continental slope show crustal refractions and interplate boundary reflections constraining the seismic structure of the continental crust and geometry of the subducting oceanic Nazca plate. Most stations provided offsets of 80-120 km. Some stations show seismic energy up to 150 km distance. Fig. 5.13b shows an example record section of OBS206 (hydrophone component).

5.3.4.4 3D experiment

First results of the 3D experiment indicate a dense ray coverage through the entire network with sedimentary phases of up to 1.5 km thickness, crustal phases from the overriding continental plate and wide-angle reflections from the subducting plate. A data example is shown in Fig. 5.14. Within the 3D experiment, the shot interval was 60 s for most of the profiles. During a short period, only the half airgun array was used, and the shot interval was lowered to 10 s (first traces in Fig. 5.14).

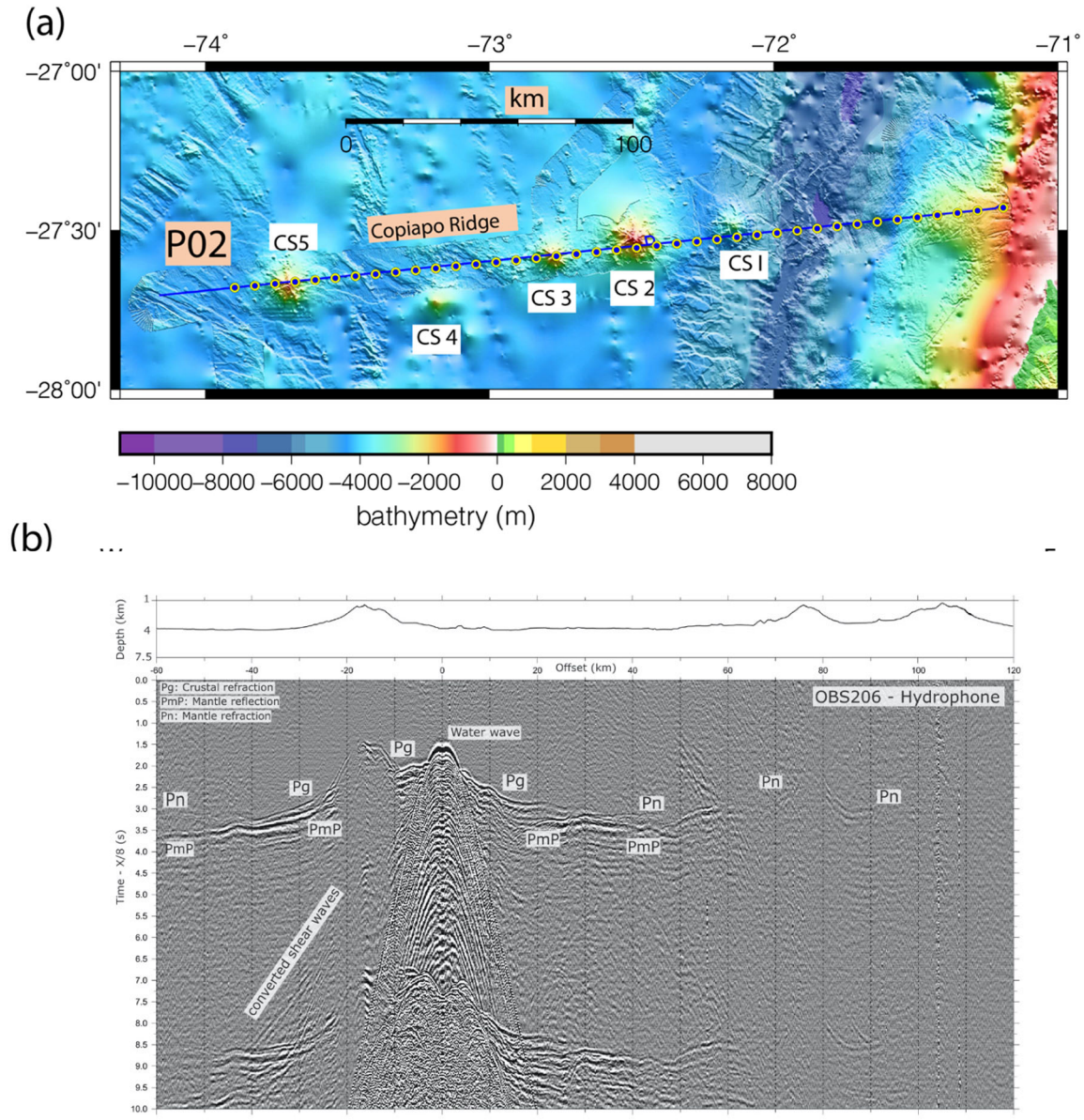

Fig. 5.13 (a) Swath bathymetric image of the seafloor off Atacama region, northern Chile. The Copayapu seamounts I-IV (CS I-V) correspond to the easternmost portion of the Copiapó Ridge before the collision with the continental South American plate (Contreras-Reyes & Carrizo, 2011). Black line denotes the wide-angle seismic profile p200. Dots correspond to the deployed 39 OBH/S (b) Hydrophone component of OBS206 on the oceanic plate.

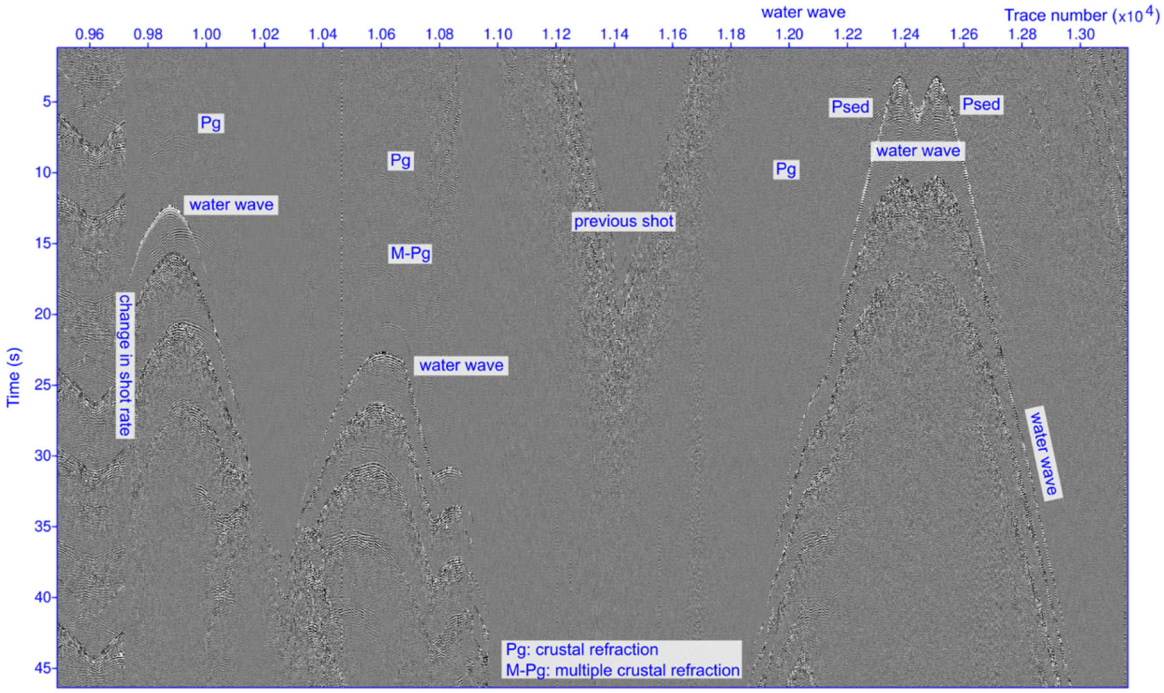

Fig. 5.14 Data example from the 3D experiment on the forearc, showing a shot section of the hydrophone component of OBS 3B01 filtered with a band pass filter (1, 4, 20, 30 Hz).

5.3.4.5 Anisotropy experiment

The anisotropy study aims to improve our understanding of in-situ properties beyond the seismic velocity of the oceanic crust. These data may provide intrinsic properties such as structural features, faults, micro-fracturing or the in-situ stress and strain of the upper crust that will be subducted in the geologically near future. Reaching the upper mantle in such an experiment would require substantial shooting offsets (~30 km) and a directed source, which is not feasible in this experiment.

Three circles have been shot around an array of 4 OBS and 1 OBH in a distance of 3 nm, 5 nm and 8 nm, respectively (blue circles in map, Fig. 5.3.1). Refracted phases of different depth levels have been recorded. In Fig. 5.15, a data example of the hydrophone component of OBS103 is shown. All components of the deployed instruments showed data with a high signal-to-noise ratio. The airgun was not directed towards the OBS, resulting in weaker first arrivals at 8 nm compared to the usual energy recorded on stations along a profile; compare to Fig. 5.13 at the same offset on the oceanic plate. Changes in the amplitude of the hydrophone component are visible and hint at changes in the upper crust structure depending on the azimuth.

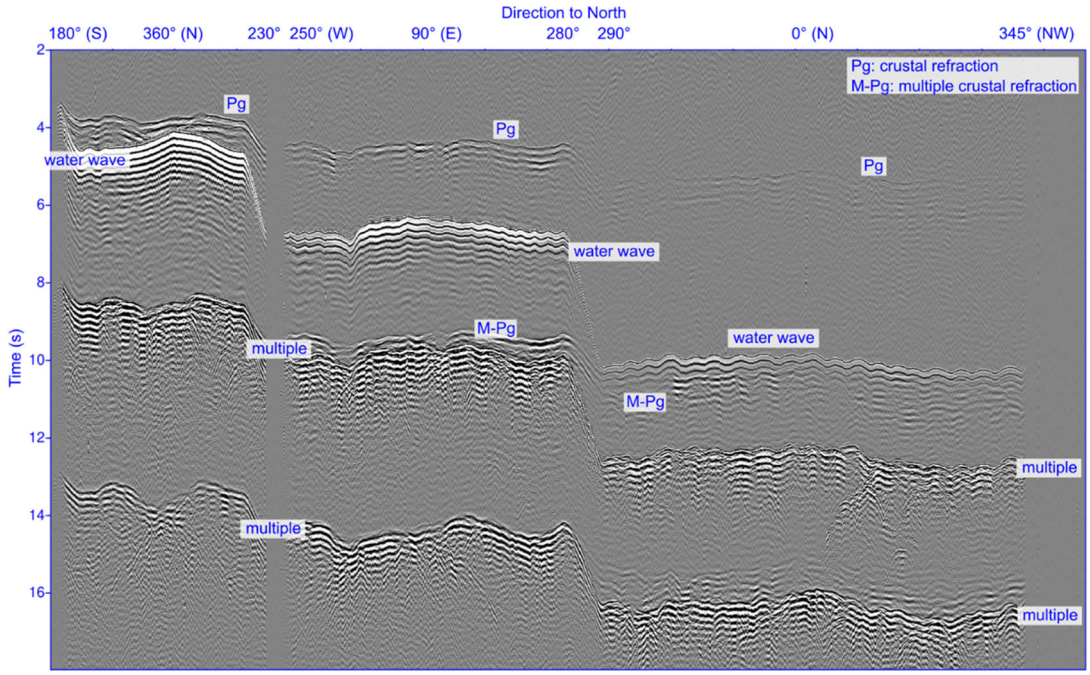

Fig. 5.15 Shot section of OBS103 located in the centre of the shot circles. Here the hydrophone component is shown, unprocessed with a bandpass filter (1,4,20,30 Hz).

5.4 CTD Measurements

During SO297, a total of 4 vertical profiles of pressure (P), temperature (T), conductivity (C) and oxygen (O) were recorded. The CTD/O2 profiles ranged from the surface up to 2496 m depth (Tab. 6.4). We used the ship's CTD system attached to the water sampler carousel, and SBE Seasave software. The CTD system performed without problems throughout the whole cruise.

5.5. Expected Results

We expect to generate seismic 2D P-wave velocity models along the two transects from the oceanic plate in the west, crossing the trench and covering the overriding plate in the offshore region in the east. The geometry of the plate interface between the subducting and the overriding plate is indicated by reflections in the OBS data. We expect to receive an entire image of the subduction zone along the two volcanic ridges, Copiapó Ridge and Taltal Ridge. The first results from forward modelling show the oceanic crust to be 10-15% thicker than "normal" oceanic crust (Fig. 5.5.1). This is in good agreement with the graben structures observed in the bathymetric data and MCS data. From the 3D array, we expect seismic velocity models that cross the Taltal Ridge in the trench, providing information on the width of the ridge. The analysis of the 3D network aims to shed light on the influence of the volcanic ridge on the subduction process. Additionally, observed converted shear-waves will contribute to understanding the crustal anisotropy and possibly the stress regime. They will be used to analyse the petrology of the subducting plate.

The high-resolution structural images obtained in this project, together with data from the IPOC and the 55 temporal seismic stations IMO and GEOMAR installed onshore, will be used to investigate the control of upper and lower plate structure on slip, coupling and other rheological parameters. The 2D- and 3D seismic survey acquired during the SO207 cruise was designed to elucidate the geometry of rupture domains, which is a prerequisite to better comprehending co-

seismic slip propagation and the potential size of future earthquakes. The ultimate goal of the 3D refraction experiment is to resolve and better understand along-strike variations of the forearc and incoming plate and their relation to rupture domains

The multibeam data revealed a significant region of previously uncharted seafloor. In particular, we will further investigate the graben structures and their relation to the Taltal Ridge. This will be done by comparing the different datasets such as MCS and refraction models, with the PARASOUND and Multibeam.

The five novel pressure sensors installed during SO297 will allow resolving pressure changes without drift and hence sea-level changes and subsidence of the oceanic plate and marine forearc with a cm precision. The first 10 days of data downloaded during the cruise shows that the temperature and inclination of station PRS1 are possibly related to pressure changes and tidal driven currents at the seafloor. The pressure instruments will remain between 2 and 5 years on the seafloor, and future uploads of the data from the seafloor will reveal longer time-series.

The high-resolution structural information of the Chilean subduction zone will significantly improve our knowledge of the offshore part of the erosive margin in North-Central Chile, where only limited information has been available to date. This lack of knowledge was in contrast to the rich observations on land. The newly acquired data during SO297 will help to better understand the entire subduction system. Since erosive margins are capable of producing very large earthquakes (as the Tohoku 2011 earthquake documented) a better understanding of how upper and lower plate structure are related to the distribution of slip before, during and after large earthquakes is a prerequisite to thoroughly assess earthquake rupture and slip distribution.

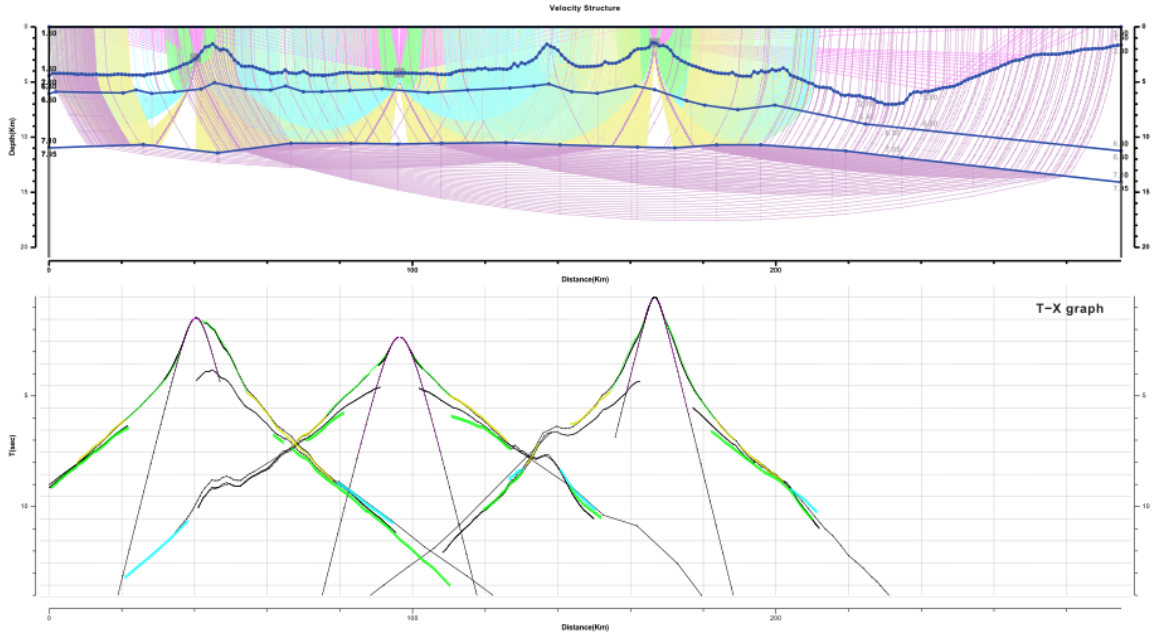

Fig. 5.16 Preliminary forward model using rayinvr (Zelt et al., 1999) for the western part (180 km long) of profile P200 (upper panel). For clarity, three of the 20 picked OBS/OBH are shown in the lower panel.

6 Station List SO297

6.1 Overall Station Lists

Tab. 6.1 List of 116 installed OBS/OBH (including the coordinates of the two lost OBH), four CTD measurements and five pressure moorings. Station coordinates correspond to the deployment coordinates of DSHIP.

Station No.	Date	Gear	Time	Latitude	Longitude	Water Depth	Name/
	2023		[UTC]	[°N]	[°W]	[m]	Remarks
SO297_1-2	26.02.	CTD	02:33	30°59.90'	73°39.76'	2500	CTD
SO297_2-1	27.02.	OBS	03:47	27°40.86'	73°53.81'	4330.6	P201
SO297_3-1	27.02.	OBS	04:34	27°40.47'	73°49.55'	3933.3	P202
SO297_4-1	27.02.	OBS	05:21	27°40.12'	73°45.22'	3045.5	P203
SO297_5-1	27.02.	OBH	06:02	27°39.77'	73°41.08'	1952.2	P204
SO297_6-1	27.02.	OBS	06:47	27°39.39'	73°36.87'	3560.6	P205
SO297_7-1	27.02.	OBS	07:31	27°39.04'	73°32.56'	4199.3	P206
SO297_8-1	27.02.	OBS	08:11	27°38.68'	73°28.31'	4126.5	P207
SO297_9-1	27.02.	OBS	08:43	27°38.30'	73°24.03'	4400.7	P208
SO297_10-1	27.02.	OBS	09:14	27°37.95'	73°19.80'	4126.1	P209
SO297_11-1	27.02.	OBS	09:45	27°37.59'	73°15.56'	4176.8	P210
SO297_12-1	27.02.	OBS	10:17	27°37.26'	73°11.31'	4181.0	P211
SO297_13-1	27.02.	OBS	10:50	27°36.86'	73°07.10'	4202.3	P212
SO297_14-1	27.02.	OBS	11:22	27°36.47'	73°02.83'	4291.6	P213
SO297_15-1	27.02.	OBS	11:52	27°36.10'	72°58.56'	3814.2	P214
SO297_16-1	27.02.	OBS	12:22	27°35.77'	72°54.35'	3778.7	P215
SO297_17-1	27.02.	OBS	12:54	27°35.37'	72°50.08'	3220.7	P216
SO297_18-1	27.02.	OBH	13:23	27°35.00'	72°45.83'	1711.5	P217 - lost
SO297_19-1	27.02.	OBH	13:56	27°34.62'	72°41.63'	3556.0	P218
SO297_20-1	27.02.	OBH	14:26	27°34.22'	72°37.40'	3178.5	P219
SO297_21-1	27.02.	OBH	14:58	27°33.77'	72°33.21'	2733.4	P220
SO297_22-1	27.02.	OBH	15:27	27°33.37'	72°28.94'	1454.4	P221
SO297_23-1	27.02.	OBH	15:58	27°33.00'	72°24.67'	2928.6	P222
SO297_24-1	27.02.	OBS	16:34	27°32.57'	72°20.48'	3920.1	P223
SO297_25-1	27.02.	OBS	17:09	27°32.16'	72°16.21'	4086.8	P224
SO297_26-1	27.02.	OBS	17:46	27°31.75'	72°11.97'	4347.5	P225
SO297_27-1	27.02.	CTD	18:02	27°31.85'	72°11.41'	2500	CTD
SO297_28-1	27.02.	OBS	20:52	27°31.37'	72°07.68'	4316.1	P226
SO297_29-1	27.02.	OBS	21:33	27°30.95'	72°03.44'	5089.1	P227
SO297_30-1	27.02.	OBS	22:18	27°30.53'	71°59.08'	5718.9	P228
SO297_31-1	27.02.	OBS	22:56	27°30.17'	71°54.94'	6211.6	P229
SO297_31-1	27.02.	OBS	23:35	27°30.14'	71°55.01'	6109.2	P229
SO297_32-1	28.02.	OBS	00:18	27°29.65'	71°50.77'	7011.9	P230
SO297_33-1	28.02.	OBS	00:55	27°29.32'	71°46.54'	6095.9	P231
SO297_34-1	28.02.	OBS	01:38	27°28.96'	71°42.33'	5716.0	P232
SO297_35-1	28.02.	OBS	02:16	27°28.53'	71°38.08'	5179.4	P233
SO297_36-1	28.02.	OBS	02:55	27°28.09'	71°33.85'	5069.2	P234
SO297_37-1	28.02.	OBH	03:34	27°27.64'	71°29.61'	3111.8	P235
SO297_38-1	28.02.	OBH	04:15	27°27.19'	71°25.44'	2558.6	P236
SO297_39-1	28.02.	OBH	05:00	27°26.78'	71°21.20'	2451.7	P237
SO297_40-1	28.02.	OBH	05:44	27°26.32'	71°17.01'	2019.1	P238
SO297_41-1	28.02.	OBS	06:31	27°25.80'	71°12.07'	1675.9	P239
SO297_83-1	06.03.	OBS	03:33	26°01.37'	71°15.62'	4617.1	3B13
SO297_84-1	06.03.	OBS	04:48	25°51.60'	71°15.60'	5237.1	3B11
SO297_85-1	06.03.	OBS	06:36	25°37.24'	71°21.55'	7132.2	3A09
SO297_86-1	06.03.	OBS	07:32	25°30.02'	71°21.61'	5801.3	3A08

SO297_87-1	06.03.	OBS	08:25	25°30.00'	71°29.41'	7143.2	OF01
SO297_88-1	06.03.	OBS	09:37	25°22.78'	71°37.82'	6262.5	P2X1
SO297_89-1	06.03.	OBS	10:09	25°22.77'	71°33.55'	7196.2	P2X2
SO297_90-1	06.03.	OBS	10:38	25°22.79'	71°29.39'	7309.5	P2X3
SO297_91-1	06.03.	OBS	11:08	25°22.77'	71°25.21'	6515.4	P2X4
SO297_91-2	06.03.	CTD	12:27	25°22.76'	71°25,17'	2500	CTD
SO297_92-1	06.03.	OBS	15:09	25°22.80'	71°15.64'	4900.3	3B07
SO297_93-1	06.03.	OBS	16:06	25°15.55'	71°15.65'	5450.3	3B06
SO297_94-1	06.03.	OBS	17:11	25°15.58'	71°25.19'	6837.6	OF02
SO297_95-1	06.03.	OBS	18:17	25°08.47'	71°20.44'	7805.0	3A05
SO297_96-1	06.03.	OBS	18:58	25°08.36'	71°15.62'	7357.9	3B05
SO297_97-1	06.03.	OBS	19:52	25°01.22'	71°15.60'	7677.1	3B04
SO297_98-1	06.03.	OBS	20:36	24°54.59'	71°15.59'	7658.0	3B03
SO297_99-1	06.03.	OBS	21:48	24°44.39'	71°15.64'	5246.8	3B01
SO297_100-1	06.03.	OBS	23:13	24°54.59'	71°08.40'	4213.4	3C03
SO297_101-1	07.03.	OBS	00:04	25°01.15'	71°08.38'	4066.1	3C04
SO297_102-1	07.03.	OBH	01:01	25°01.19'	71°01.21'	3364.8	3D04
SO297_103-1	07.03.	OBH	02:04	25°08.38'	71°01.16'	3121.7	3D05
SO297_104-1	07.03.	OBH	03:01	25°08.40'	70°54.00'	2367.9	3E05
SO297_105-1	07.03.	OBH	04:22	25°15.56'	70°46.80'	1648.8	3F06
SO297_106-1	07.03.	OBH	05:36	25°15.61'	70°54.08'	2278.3	3E06
SO297_107-1	07.03.	OBH	06:31	25°15.59'	71°01.21'	3109.4	3D06
SO297_108-1	07.03.	OBS	07:54	25°08.31'	71°08.44'	4323.6	3C05
SO297_109-1	07.03.	OBS	08:57	25°15.59'	71°08.41'	4127.9	3C06
SO297_110-1	07.03.	OBS	09:54	25°22.80'	71°08.39'	4081.6	3C07
SO297_111-1	07.03.	OBS	10:51	25°22.84'	71°01.22'	3544.3	3D07
SO297_112-1	07.03.	OBS	11:48	25°22.82'	70°54.00'	2230.3	3E07
SO297_113-1	07.03.	OBH	12:27	25°22.79'	70°50.25'	1614.2	P1X5
SO297_114-1	07.03.	OBH	13:23	25°29.71'	70°53.85'	2214.9	3E08
SO297_115-1	07.03.	OBH	14:18	25°30.03'	71°01.15'	3598.6	3D08
SO297_116-1	07.03.	OBS	15:07	25°30.14'	71°08.47'	4254.2	3C08
SO297_117-1	07.03.	OBS	15:52	25°30.11'	71°15.57'	4826.1	3B08
SO297_118-1	07.03.	OBS	16:43	25°37.12'	71°15.56'	4861.5	3B09
SO297_119-1	07.03.	OBS	17:35	25°44.32'	71°15.61'	4673.8	3B10
SO297_120-1	07.03.	OBH	18:26	25°44.26'	71°08.53'	3662.6	3C10
SO297_121-1	07.03.	OBS	19:22	25°37.16'	71°08.44'	4178.1	3C09
SO297_122-1	07.03.	OBH	20:11	25°37.18'	71°01.19'	2863.1	3D09
SO297_123-1	07.03.	OBS	20:48	25°37.19'	70°55.78'	2030.3	3E09
SO297_124-1	07.03.	OBS	21:01	25°38.09'	70°56.12'	1904.6	3D10 Lost
SO297_130-1	17.03.	CTD	09:22	24°56.20'	70°53,50'	1700	CTD
SO297_131-1	17.03.	PRS1	16:38	24°56.20’	70°53.49’	1785.0	Deployed, IMO, 1903
SO297_133-1	19.03.	PRS3	17:41	24°55.00'	71°21.10’	5961.0	Deployed, IMO, 1902
SO297_147-1	21.03.	PRS2	12:16	24°56.00’	71°11.80’	4449.0	Deployed, IMO, 1901
SO297_160-1	22.03.	OBS	15:25	25°22.75'	71°21.00'	5821.3	P133
SO297_161-1	22.03.	OBS	15:51	25°22.78'	71°18.05'	5376.8	P134
SO297_162-1	22.03.	OBS	16:35	25°22.79'	71°12.02'	4501.2	P136
SO297_163-1	22.03.	OBS	17:26	25°22.77'	71°04.83'	3956.0	P138
SO297_164-1	22.03.	OBS	18:16	25°22.79'	70°57.61'	3019.7	P140
SO297_173-1	23.03.	OBS	10:53	25°22.78'	71°41.99'	5955.1	P128
SO297_174-1	23.03.	OBS	11:20	25°22.81'	71°45.45'	5386.8	P127
SO297_175-1	23.03.	OBS	11:52	25°22.81'	71°49.64'	5001.0	P126
SO297_176-1	23.03.	OBS	12:26	25°22.78'	71°53.87'	4523.9	P125
SO297_177-1	23.03.	OBS	12:58	25°22.78'	71°57.96'	4283.0	P124
SO297_178-1	23.03.	OBS	13:28	25°22.76'	72°02.20'	4242.9	P123

SO297_179-1	23.03.	OBS	14:04	25°22.82'	72°06.34'	3982.6	P122
SO297_180-1	23.03.	OBH	14:40	25°22.80'	72°10.55'	3348.3	P121
SO297_181-1	23.03.	OBH	15:18	25°22.81'	72°14.72'	3161.5	P120
SO297_182-1	23.03.	OBH	16:05	25°22.79'	72°18.95'	3306.8	P119
SO297_183-1	23.03.	OBS	16:48	25°22.77'	72°23.10'	3990.9	P118
SO297_184-1	23.03.	OBS	17:34	25°22.79'	72°27.30'	4214.6	P117
SO297_185-1	23.03.	OBS	20:09	25°22.80'	72°31.49'	4206.1	P116
SO297_186-1	23.03.	OBS	20:53	25°22.80'	72°35.69'	4107.6	P115
SO297_187-1	23.03.	OBS	21:36	25°22.78'	72°39.84'	3810.2	P114
SO297_188-1	23.03.	OBS	22:14	25°22.78'	72°43.42'	3242.3	P113
SO297_189-1	23.03.	OBS	22:43	25°22.79'	72°46.13'	2592.8	P112
SO297_190-1	23.03.	OBS	23:07	25°22.77'	72°48.22'	1901.9	P111
SO297_191-1	23.03.	OBS	23:37	25°22.78'	72°50.79'	1131.0	P110
SO297_192-1	24.03.	OBS	00:13	25°22.81'	72°52.44'	1414.5	P109
SO297_193-1	24.03.	OBH	00:56	25°22.80'	72°54.54'	2268.4	P108
SO297_194-1	24.03.	OBH	01:44	25°22.82'	72°57.12'	3013.0	P107
SO297_195-1	24.03.	OBH	02:43	25°22.78'	73°00.58'	3597.9	P106
SO297_196-1	24.03.	OBS	03:26	25°22.77'	73°04.88'	3963.0	P105
SO297_197-1	24.03.	OBS	04:11	25°22.79'	73°09.06'	3964.9	P104
SO297_198-1	24.03.	OBS	05:00	25°22.79'	73°13.21'	3807.6	P103
SO297_199-1	24.03.	OBH	05:47	25°22.81'	73°17.42'	4232.5	P102
SO297_231-1	28.03.	OBS	09:31	25°21.75'	73°13.26'	3810.0	P100
SO297_232-1	28.03.	OBS	09:58	25°23.77'	73°13.27'	3820.1	P101
SO297_250-1	31.03.	PRS4	16:32	24°55.90’	71°38.73’	5480.0	Deployed, GEOMAR, 1905
SO297_251-1	01.04.	PRSS	15:46	25°40.50’	71°13.01’	4598.0	Deployed, GEOMAR, 1904

6.2 Profile Station List

Tab. 6.2 Table with seismic refraction and MCS profiles aquired during SO297.

Line No.	Date Start	Time Start	Date End	Time End	Longitude Start	Latitude	Longitude	Latitude End	FFN Start	FFN End
SO 297	2023	UTC	2023	UTC	[°W]	[°S]	[°W]	[°S]		
1001	28.02.	23:56:00.050	01.03.	14:54:00.050	-71.19629736	-27.4275692	-72.44556168	-27.54642409	171	1069
1002	01.03.	15:47:00.050	02.03.	12:13:00.050	-72.45102481	-27.52152041	-74.16173355	-27.7056959	1122	2348
2001	07.03.	22:50:00.050	08.03.	03:25:00.050	-70.97266273	-25.72759780	-71.35288273	-25.73748668	3035	3310
2002	08.03.	03:26:00.050	08.03.	05:03:00.050	-71.35402382	-25.73667164	-71.35409518	-25.62313860	3311	3408
2003	08.03.	05:04:00.050	08.03.	10:48:00.050	-71.35305757	-25.62251487	-70.93483468	-25.61837985	3409	3753
2004	08.03.	10:49:00.050	08.03.	12:25:00.050	-70.93370351	-25.61779670	-70.90561940	-25.50753968	3754	3850
2005	08.03.	12:26:00.050	08.03.	18:39:00.050	-70.90639823	-25.50644926	-71.48629964	-25.49986017	3851	4224
2006	08.03.	19:36:00.050	08.03.	20:30:00.050	-71.55275583	-25.44620395	-71.60807862	-25.39402657	4281	4335
2007	08.03.	20:31:00.050	09.03.	06:05:00.050	-71.60802649	-25.39283679	-70.84371400	-25.37946828	4336	4910
2008	09.03.	06:06:00.050	09.03.	07:45:00.050	-70.84237432	-25.37919730	-70.78975188	-25.26748032	4911	5010
2009	09.03.	07:46:00.050	09.03.	10:59:00.050	-70.7904343	-25.26646606	-71.05738378	-25.2600580	5011	5204
2010	09.03.	12:00:00.050	09.03.	12:47:00.050	-71.14119179	-25.25996026	-71.14284003	-25.23549426	5265	5312
2011	09.03.	13:35:00.050	09.03.	18:14:00.050	-71.17024677	-25.26145048	-71.53312885	-25.25992859	5360	5639

2012	09.03.	18:36:00.050	09.03.	19:11:00.050	-71.55915571	-25.25009483	-71.55997654	-25.20434875	5661	5696
3001	09.03.	20:22:30.050	09.03.	22:06:36.050	-71.55954290	-25.12958931	-71.55680165	-25.00435997	6103	6450
3002	09.03.	22:06:54.050	10.03.	06:36:36.050	-71.55654155	-25.00406891	-70.81906644	-24.99691158	6451	8150
3003	10.03.	06:36:54.050	10.03.	08:03:36.050	-70.81877907	-24.99669057	-70.82242606	-24.90662969	8151	8440
3004	10.03.	08:03:54.050	10.03.	12:00:36.050	-70.82279282	-24.90650985	-71.11554187	-24.90506150	8441	9230
4001	10.03.	13:55:48.050	10.03.	18:40:48.050	-71.17728103	-24.91906693	-71.54552856	-24.91081946	10100	11050
4002	10.03.	18:41:06.050	10.03.	19:20:42.050	-71.5457171	-24.91117883	-71.49909960	-24.92528371	11051	11183
5001	10.03.	20:10:00.050	11.03.	03:58:00.050	-71.47323875	-24.89600359	-70.81679972	-24.90953202	12012	12480
5002	11.03.	03:59:00.050	11.03.	05:13:00.050	-70.81590462	-24.91056632	-70.81363438	-25.01000348	12481	12555
5003	11.03.	05:14:00.050	11.03.	12:08:00.050	-70.81406638	-25.01131276	-71.33160358	-25.02325224	12556	12970
5004	11.03.	12:09:00.050	11.03.	13:43:00.050	-71.33252484	-25.02403519	-71.33365541	-25.13744793	12971	13065
5005	11.03.	13:44:00.050	11.03.	15:24:00.050	-71.33242341	-25.13818873	-71.18094511	-25.14003700	13066	13166
5006	11.03.	16:41:00.050	11.03.	17:19:00.050	-71.07014765	-25.13998987	-71.01599756	-25.13988717	13243	13281
5007	11.03.	18:14:00.050	11.03.	19:05:00.050	-70.93796064	-25.14000861	-70.86863075	-25.13998310	13286	13337
5008	11.03	19:46:00.050	11.03.	19:54:00.050	-70.85218392	-25.17377158	-70.85740609	-25.18327600	13340	13348
5009	11.03.	20:22:00.050	11.03.	20:30:00.050	-70.87583485	-25.21648895	-70.88097638	-25.22582995	13353	13361
5010	11.03.	21:11:00.050	11.03.	21:45:00.050	-70.8998549	-25.27356593	-70.90176061	-25.31680439	13364	13398
5011	11.03.	21:46:00.050	11.03.	22:26:00.050	-70.90268587	-25.31787820	-70.95999350	-25.32073506	13399	13439
5012	11.03.	22:52:00.050	11.03.	23:32:00.050	-70.99557852	-25.32063846	-71.04505690	-25.32652295	13465	13505
5013	11.03.	23:33:00.050	12.03.	04:44:00.050	-71.04559300	-25.32751215	-71.01086090	-25.72455464	13506	13817
5014	12.03.	04:45:00.050	12.03.	07:52:00.050	-71.00956791	-25.72502575	-70.90055644	-25.52924067	13818	14005
5015	12.03.	07:53:00.050	12.03.	12:25:00.050	-70.90046096	-25.52802909	-70.90157295	-25.20630036	14006	14278
5016	12.03.	12:26:00.050	12.03.	13:09:00.050	-70.90230949	-25.20534537	-70.95745520	-25.19999447	14279	14322
5017	12.03.	13:21:00.050	12.03.	13:44:00.050	-70.97043180	-25.19241773	-70.99279128	-25.17220279	14334	14357
5018	12.03.	14:11:00.050	12.03.	15:47:00.050	-71.01801179	-25.14894294	-71.02042215	-25.02831959	14384	14480
5019	12.03.	15:48:00.050	12.03.	17:17:00.050	-71.02093387	-25.02716464	-71.13406458	-25.01822776	14481	14570
5020	12.03.	17:18:00.050	12.03.	20:22:00.050	-71.13517269	-25.01747468	-71.25969543	-24.81920218	14571	14755
5021	12.03.	20:23:00.050	12.03.	22:27:00.050	-71.25985051	-24.8179639	-71.24290493	-24.67790890	14756	14880
5022	12.03.	22:28:00.050	13.03.	16:19:00.050	-71.24177074	-24.67837879	-71.2562860	-26.07386228	14881	15952
5023	13.03.	17:53:00.050	13.03.	20:22:00.050	-71.14109627	-26.06351199	-71.13998251	-25.88774707	15956	16105
5024	13.03.	20:47:00.050	13.03.	22:20:00.050	-71.14011710	-25.85674707	-71.13596481	-25.74407006	16130	16223
5025	13.03.	22:21:00.050	14.03.	00:11:00.050	-71.13505801	-25.74330882	-70.9871708	-25.73697497	16224	16334
5026	14.03.	00:12:00.050	14.03.	08:07:00.050	-70.98619176	-25.73618076	-70.71643922	-25.24262432	16335	16810
5027	14.03.	08:08:00.050	14.03.	13:47:00.050	-70.71631496	-25.24147435	-71.0038045	-24.93272678	16811	17150
5028	14.03.	13:48:00.050	14.03.	14:57:00.050	-71.00509047	-24.93264413	-71.01991265	-25.01794782	17151	17220
5029	14.03.	15:29:00.050	14.03.	17:24:00.050	-71.01995613	-25.06070100	-71.01991076	-25.21990308	17225	17340
5030	14.03.	18:07:00.050	14.03.	18:53:00.050	-71.01992289	-25.27706101	-71.06563547	-25.30010947	17345	17391
5031	14.03.	20:00:00.050	15.03.	01:02:00.050	-71.0815171	-25.23387189	-71.08739742	-24.87956009	17458	17760
5032	15.03.	01:03:00.050	15.03.	01:37:00.050	-71.08841266	-24.87895500	-71.13252363	-24.87799270	17761	17795

5033	15.03.	01:38:00.050	15.03.	12:03:00.050	-71.13362553	-24.87860465	-71.14002060	-25.68851608	17796	18420
5034	15.03.	12:44:00.050	15.03.	14:31:00.050	-71.16770323	-25.69892108	-71.14003527	-25.78841800	18430	18537
6001	17.03.	22:13:00.050	18.03.	11:33:00.050	-71.36017242	-24.85782945	-71.36009088	-25.9233197	19009	19809
6002	18.03.	11:46:00.050	18.03.	12:55:00.050	-71.35999167	-25.94011500	-71.35948000	-26.02211000	-	-
6003	18.03.	13:14:00.050	19.03.	10:55:00.050	-71.35301333	-26.03475167	-71.35236333	-24.91589167	-	-
7001	19.03.	21:31:00.050	20.03.	13:35:00.050	-71.34824833	-24.95518333	-71.19501667	-25.84987667	-	-
8001	24.03.	13:12:00.050	24.03.	14:15:00.050	-73.35496834	-25.29754853	-73.37114692	-25.37301258	20009	20071
8002	24.03.	14:16:00.050	24.03.	18:16:00.050	-73.37033475	-25.37399595	-73.04182592	-25.37991493	20072	20312
8003	24.03.	18:49:00.050	24.03.	23:50:00.050	-73.02969345	-25.40689125	-72.75744054	-25.40949783	20345	20646
8004	24.03.	23:51:00.050	25.03.	13:50:00.050	-72.75907606	-25.40927645	-71.71128347	-25.38002461	20647	21486
8005	25.03.	14:34:00.050	25.03.	15:26:00.050	-71.71742425	-25.35519982	-71.68545487	-25.37993891	21487	21539
8006	25.03.	16:00:00.050	25.03.	16:57:00.050	-71.67385664	-25.40504895	-71.66812839	-25.37977711	21573	21630
8007	25.03.	17:31:00.050	25.03.	18:27:00.050	-71.64559333	-25.40271207	-71.66572608	-25.38127269	21664	21720
8008	25.03.	19:01:00.050	26.03.	05:00:00.050	-71.61828982	-25.37999500	-70.81899609	-25.37825943	21725	22324
9001	26.03.	05:09:20.050	26.03.	06:21:50.050	-70.81089238	-25.36970125	-70.81135465	-25.36116384	23017	23450
9002	26.03.	06:22:00.050	26.03.	11:56:36.050	-70.81127880	-25.36134116	-71.25375796	-25.38007132	23451	25174
Aniso.	28.03.	14:54:00.050	29.03.	16:45:00.050	-73.22373920	-25.41525445	-73.32533163	-25.28696148	-	-

7 Data and Sample Storage and Availability

The metadata of the onboard DSHIP-System is collected and made publicly available through the Kiel Data Management Team (KDMT), which provides an information and data archival system. This Ocean Science Information System (OSIS-Kiel) is accessible to all project participants and can be used to share and edit field information and to provide scientific data as they become available. The central system OSIS is providing information on granted ship time with information on the scientific program and the general details down to the availability of data files from already concluded cruises. The transparency on the research activities is regarded as an invitation to external scientists to start communication on collaboration on behalf of the newly available data.

The KDMT will take care as data curators to fulfil the here proposed data publication of the data in a World Data Center (e.g. PANGAEA), which will then provide long-term archival and access to the data. The data publication process will be based on the available files in OSIS and is, therefore, transparent to all reviewers and scientists. This cooperation with a world data center will make the data globally searchable, and links to the data owners will provide points of contact to project-external scientists. The seismic, bathymetric and hydro-acoustic raw data and video footage, as well as processed seismic data, will be archived on a dedicated server at GEOMAR, which is daily backed up and which holds all data since the founding days of GEOMAR. OSIS provides contact information for these large data files.

Availability of metadata in OSIS-Kiel(portal.geomar.de/osis): 2 weeks after the cruise

Availability of data in OSIS-Kiel (portal.geomar.de/osis): 6 months after the cruise

Availability of data in a WDC/PANGAEA (www.pangaea.de): 5 years after the cruise

All hydroacoustic data collected during SO297 are stored in facilities of GEOMAR Helmholtz-Zentrum für Ozeanforschung Kiel (responsible Dr. D. Lange). Multibeam field data are stored at the bathymetric data centre of the Bundesamt für Seeschiffahrt und Hydrografie.

Tab. 7.1 Overview of data availability.

Type	Database	Available	Free Access	Contact
CTD	PANGEA	July 2022	May 2028	dlange@geomar.de
EM122 Multibeam	BSH, PANGAEA	July 2022	May 2028	iklaucke@geomar.de
PARASOUND	GEOMAR	July 2022	May 2028	dlange@geomar.de
Pressure-Sensors GEOMAR	GEOMAR	July 2022	May 2028	dlange@geomar.de
MCS Data	GEOMAR	July 2022	May 2028	dlange@geomar.de
OBS Data	GEOMAR	July 2022	May 2028	dlange@geomar.de
OBH Data	GEOMAR	July 2022	May 2028	dlange@geomar.de
Ship's Metadata	BSH, OSIS-Kiel	May 2023	May 2023	

8 Acknowledgements

The ambitious planning and preparation related to cruise SO297 of RV SONNE would not have been possible without the excellent shore-based administrative and logistical support of the Leitstelle Deutsche Forschungsschiffe, Briese Research and the Projektträger Jülich. We gratefully acknowledge the help of the Foreign Office in Berlin and the German Embassy in Santiago de Chile. We would also like to thank the Government of Chile for granting opportunity to work within their territorial waters. S.H.O.A. is thanked for the efficient permitting process. We especially thank Captain Oliver Meyer and his crew for their skillful execution of the complex scientific program and the pleasant atmosphere on board. The cruise and scientific work were financed by the Bundesministerium für Bildung und Forschung (BMBF) under grant 03G0297A (PISAGUA) with additional funding and use of large-scale equipment from GEOMAR.

9 References

Beck, S., Barrientos, S., Kausel, E., Reyes, M., 1998. Source characteristics of historic earthquakes along the central Chile subduction zone. Journal of South American Earth Sciences 11, 115–129. https://doi.org/10.1016/S0895-9811(98)00005-4

Bialas, J., and Flueh, E.R., 1999. Ocean Bottom Seismometers, Sea Technology, 40, 4, 41-46, 1999.

Bilek, S.L., 2010. The role of subduction erosion on seismicity. Geology 38, 479–480. doi:10.1130/focus052010.1

Clift, P., Vannucchi, P., 2004. Controls on tectonic accretion versus erosion in subduction zones: Implications for the origin and recycling of the continental crust. Rev. Geophys. 42, RG2001. doi:10.1029/2003RG000127.

Collings, R., Lange, D., Rietbrock, A., F. Tilmann, D. Natawidjaja, B. Suwargadi, M. Miller, und J. Saul, 2012. Structure and seismogenic properties of the Mentawai segment of the Sumatra subduction zone revealed by local earthquake traveltime tomography. Journal of Geophysical Research 117: 23, doi:201210.1029/2011JB008469.

Contreras-Reyes, E., and D. Carrizo, 2011. Control of high oceanic features and subduction channel on earthquake ruptures along the Chile–Peru subduction zone, Phys. Earth Plan. Int., v. 186, 49-58.

Contreras-Reyes, E., J. Jara, I. Grevemeyer, S. Ruiz, and D. Carrizo, 2012. Abrupt change in the dip of the subducting plate beneath north Chile, Nature Geoscience, doi:10.1038/ngeo1447.

Contreras-Reyes, E., 2018. Structure and Tectonics of the Chilean Convergent Margin from Wide-Angle Seismic Studies: A Review, in: Folguera, A., et al. (Eds.), The Evolution of the Chilean-Argentinean Andes, Springer Earth System Sciences. Springer International Publishing, Cham, pp. 3–29. https://doi.org/10.1007/978-3-319-67774-3_1

Kanamori, H., 1986. Rupture process of subduction-zone earthquakes, Annu. Rev. Earth Planet. Sci., 14, 293–322.

Kopp, H., 2013. Invited review paper: The control of subduction zone structural complexity and geometry on margin segmentation and seismicity, Tectonics, v. 589, p. 1-16.

Kopp, Heidrun et al., 2022. Conjoint Monitoring of the Ocean Bottom offshore Chile Humboldt Organic MattEr Remineralization, Cruise No. SO288, 15.01.2022 – 15.02.2022, Guayaquil (Ecuador) – Valparaiso (Chile) COMBO & HOMER. Open Access . SONNE-Berichte, SO288. Begutachtungspanel Forschungsschiffe, Bonn, 47 pp. DOI 10.3289/CR_SO288.

McCaffrey, R., 1993. On the role of the upper plate in great subduction zone earthquakes, J. Geophys. Res., 98(B7), 11,953– 11,966.

Moreno, M., et al., 2014. Locking of the Chile subduction zone controlled by fluid pressure before the 2010 earthquake, Nature Geoscience.

Oleskevich, D., R. Hyndman, and K. Wang, 1999. The updip and downdip limits to great subduction earthquakes: Thermal and structural models of Cascadia, south Alaska, SW Japan, and Chile, J. Geophys. Res., 104(B7), 14,965– 14,991.

Reichert, C., et al., 1996. Crustal investigations off- and onshore Nazca/Central Andes, CINCA, Sonne cruise 104, Leg 2, 26.08.-15.09.1995. Bundesanstalt für Geowissenschaften und Rostoffe, Hannover, Archiv-Nr.: 114767, 75 pp, https://doi.org/10.2312/cr_so104_2

Sallarès, V. and Ranero, C.R, 2005. Structure and Tectonics of the Erosional Convergent Margin off Antofagasta, North Chile (23°30′S). Journal of Geophysical Research: Solid Earth 110 (B6): B06101. doi:10.1029/2004JB003418.

Sallarès, V., Ranero, C.R., 2019. Upper-plate rigidity determines depth-varying rupture behaviour of megathrust earthquakes. Nature 1–6, doi: 10.1038/s41586-019-1784-0

Sandwell, D. T. and Smith, W.H.F., 1997. Marine Gravity from Geosat and ERS-1 Altimetry. J. Geophys. Res., 102, 10.039–10.054.

Tréhu, A.M., Vera, E., Riedel, M., 2016. PICTURES: Pisagua/Iquique crustal tomography to understand the region of the earthquake source. MGL1610 Cruise Report, https://doi.org/10.7284/907099 (No. MGL1610), Rolling Deck Repositry. Marcus G. Langseth.

Wilcock, W.S., et al., 2021. A Thirty-Month Seafloor Test of the A-0-A Method for Calibrating Pressure Gauges. Frontiers in Earth Science, 8, p.653.

Zelt, C. A., A. M. Hojka, E. R. Flueh, and K. D. McIntosh, 1999. 3D simultaneous seismic refraction and reflection tomography of wide-angle data from the central Chilean margin, Geophys. Res. Lett., 26, 2577-2580.

10 Abbreviations

CSN	Centro Sismológico National, Chile
CTD	Conductivity, Temperature, Pressure (Depth) Sensor
EM122	Multibeam system of RV Sonne
GEOMAR	Helmholtz-Zentrum für Ozeanforschung Kiel
IMO	Instituto Milenio de Oceanografía, Chile
IPOC	Integrated Plate boundary Observatory Chile, www.ipoc-network.org
MCS	Multichannel Seismic
OBH	Ocean Bottom Hydrophone
OBS	Ocean Bottom Seismometer
PRS	Absolute Pressure Sensor
PUCV	Pontificia Universidad Católica de Valparaíso, Chile
UChile	Universidad de Chile, Chile
UdeC	Universidad de Concepcion, Chile
VUA	Vrije Universiteit Amserdam, Niederlande

11 Appendices

11.1 Selected Pictures of Shipboard Operations

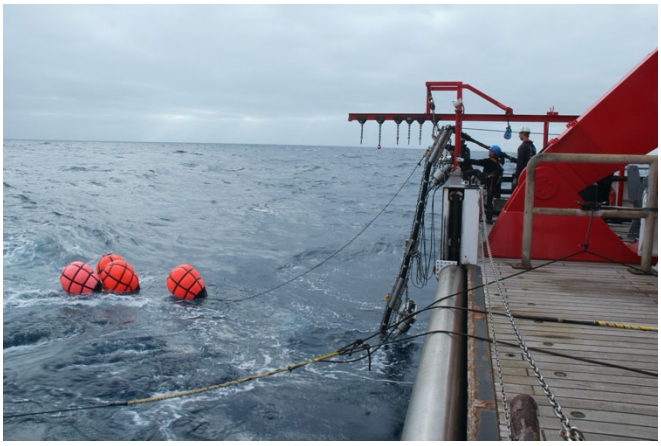

Fig. 11.1 G-gun array upon recovery.

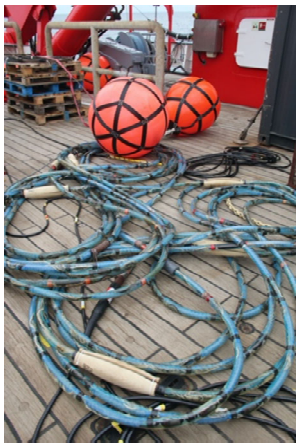

Fig. 11.2 Geometrics GeoEel Streamer segments.

Fig. 11.3 OBS before deployment.

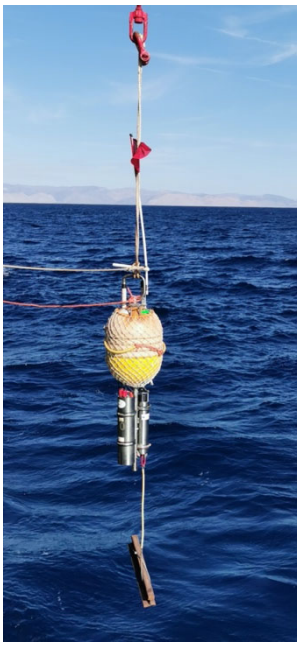

Fig. 11.4 OBH upon deployment.

Fig. 11.5 IMO Pressure sensor upon deployment.

Fig. 11.6. GEOMAR Pressure sensor mounted upon an OBS frame upon deployment.

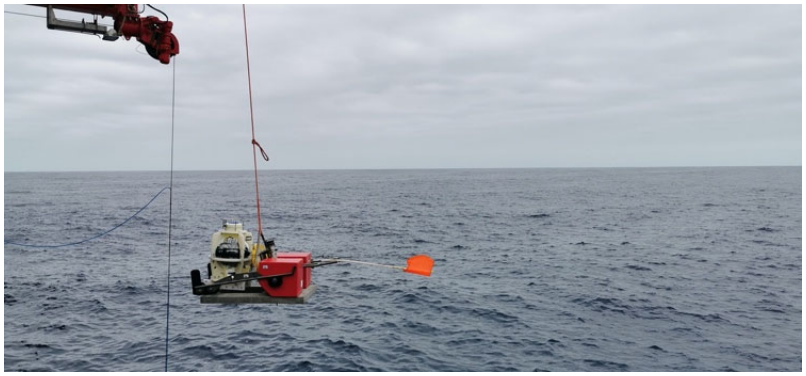

Figure 11.7 Releaser mounted on the CTD rosette for a releaser test.

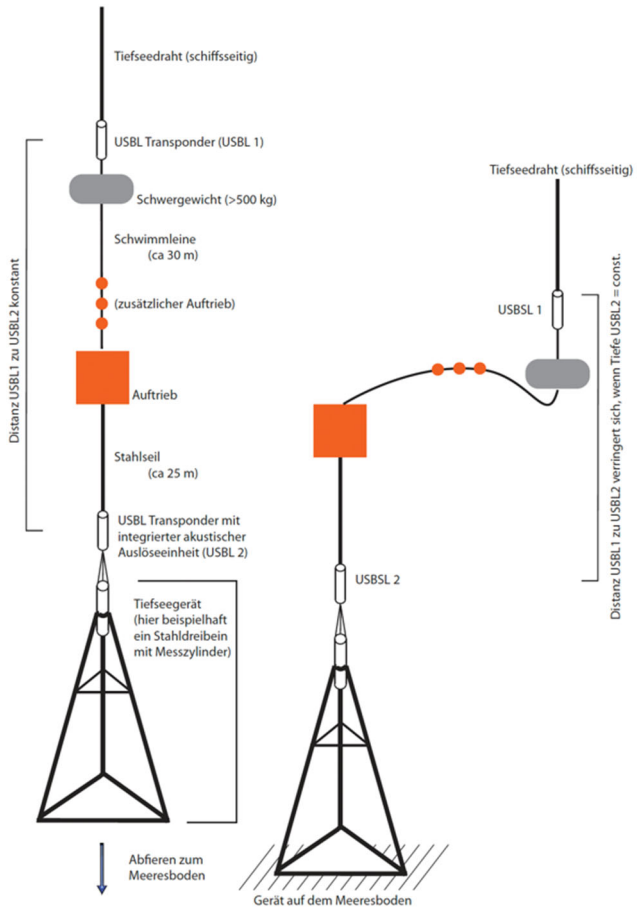

Figure 11.8 Deployment method for the absolute pressure sensor using the deep-sea cable of FS SONNE. The three Chilean instruments are installed on a tripod from Sonardyne. The two instruments from GEOMAR use an OBS rack as instrument carrier. Illustration: H. Kopp.

Fig. 11.9 Group photo of the SO297 scientific party.